

Closing the Gap Between Nano- and Macroscale: Atomic Interactions vs. Macroscopic Materials Behavior

T. Böhme¹, T. Hammerschmidt², R. Drautz² and T. Pretorius¹

¹*Dept. Research and Development, ThyssenKrupp Steel Europe AG, Duisburg*

²*Interdisciplinary Centre for Advanced Materials Simulation (ICAMS),
Ruhr-Universität Bochum
Germany*

1. Introduction

In order to meet the continuously increasing requirements in nearly all fields of technology, an ongoing development and optimization of new and existing materials, components and manufacturing facilities is necessary. The rapidly growing demand on the application side implies a constant acceleration of the complete development process. In the past, development and optimization were often based on experiments. Indeed, the efforts for this approach are mostly extensive, time consuming and expensive, which significantly restricts the development speed.

The development of numerical methods and physical models as well as steadily increasing computer capacities allow for the employment of numerical simulations during materials development and optimization. Thus the experimental efforts can be considerably reduced. Moreover, the application of computational methods allows for the investigations of physical phenomena, which are "inaccessible" from the experimental point-of-view, such as trapping behaviour of hydrogen or carbon at different lattice defects (vacancies, dislocations, grain boundaries, etc.) within an Fe-based matrix, see e.g. (Desai et al., 2010; Hristova et al., 2011; Lee, 2006; Lee & Jang, 2007; Nazarov et al., 2010).

In steel production for example, the goal is pursued to set up a so-called 'digital plant', in which it is possible to calculate the behavior of material and components up to the application level, see Figure 1. Such a digital production line provides deep insight into the materials response and the involved physical effects at each step of the process chain. Furthermore material parameters can be calculated, which will be used as input data to perform calculations of subsequently following process steps. In fact, if the production process chain can be completely reproduced, a backwards approach will be possible, which allows for the transfer from application requirements to the materials design (computer aided material design).

A fully theoretical, sufficiently accurate reproduction of all steps of materials processing is - as far as we know - still not possible. To achieve reliable simulation results in manageable computational times, (semi-)empirical models are widely used at nearly all production

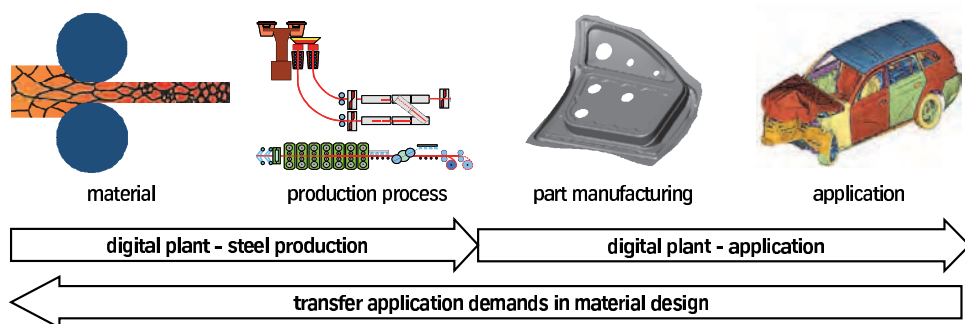


Fig. 1. Continuous full-length models of all production steps from material to application, exemplarily demonstrating materials design by simulation, e.g. during steel production.

steps. Such models make use of empirically introduced parameters, which must be fitted to experiments. For example, the description of deformation or fatigue in materials with complex microstructures, such as in multiphase steels or compound materials (e.g. fiber reinforced plastics), requires models for various physical effects on a large length- and timescale. Here, additional to macroscopic finite element analysis on the (centi-)meter scale, calculations on the microstructure (microscale) down to atomistic models (nanoscale) are necessary, cf. Figure 2.

To handle the resulting multi-scale problem, different approaches are possible. The classical approach typically starts at the application level. Here macroscopic calculations are performed, which may presuppose more detailed investigations. Such details could lead to smaller length-scales, which mainly result in an increasing number of model-parameters (input data). On the microstructure level parameters must be taken into account, in particular to describe morphology and composition as well as the temporal and spatial behaviour of the microstructures. For instance, for multiphase steels materials data of each phase and information about its shape and spatial distribution must be known. In case of compound materials the same arguments hold for the different materials fractions. Moreover, in some cases an additional description of internal interfaces (e.g. between phases or grains) must be taken into account, see for example (Artemev et al., 2000; Cahn, 1968; Kobayashi et al., 2000). By starting from the macro level, all parameters on smaller levels must be available. The efforts for the measurement of these parameters increase with decreasing length scales. Therefore, some of the required parameters cannot be measured and must be treated as fitting parameters or estimated ad hoc.

The ongoing improvement of algorithms and modeling methods accompanying the continuously rising computer capacities, allow for the use of an alternative approach to deal with the aforementioned multi-scale problems. Atomistic or even electronic level calculations can be carried out totally parameter-free (ab-initio calculations) by considering the interactions between the elemental components of matter. In this context no measurements are necessary to perform calculations at this level. Experimental data is only used for validation purposes. By following this theoretical approach, difficult experiments for the determination of required model parameters on the microscale are supplemented or partially substituted by adequate calculations. Thus, the need of fitting parameters is drastically reduced and experimental efforts are minimized, which - in turns - lead to cheaper and faster development processes.

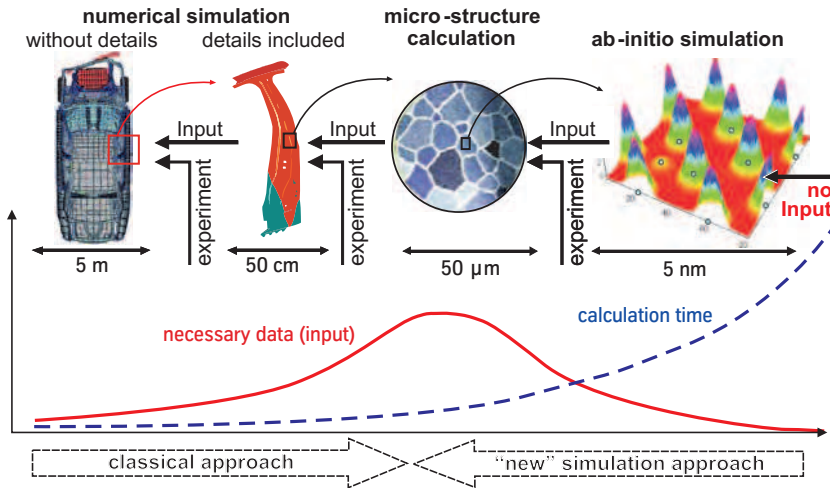


Fig. 2. Modelling on different length scales using different techniques.

However, regardless of the increasing computational capacities, most modern materials - unfortunately - are still too complex for reliable, purely-theoretical estimations of materials behaviour. Advanced high-strength steels, in particular, consist of more than 10 components (e.g. Nb, V, Al, Cr, Mn, etc.) and show different, coexisting lattice structures (e.g., martensite or austenite), orientations (texture) or precipitates (e.g., carbon nitrides). Moreover, final properties are often adjusted during advanced materials processing beyond the classical production line (e.g. annealing during surface galvanizing or hardening during hot stamping of blanks for automotive light-weight structures).

In order to understand basic mechanisms determining the specific mechanical and thermodynamic materials characteristics it is necessary to reduce the above-mentioned complexity. For this reason simple model-systems are considered to study various effects on the atomistic scale, which crucially determine the macroscopic materials properties. Recent examples in literature are e.g. binary systems such as Fe-H (Desai et al., 2010; Lee & Jang, 2007; Nazarov et.al., 2010; Psiachos et al., 2011), Fe-C (Hristova et al., 2011; Lee, 2006) or the eutectic, binary brazing alloy Ag-Cu (Böhme et al., 2007; Feraoun et al., 2001; Najababadi et al, 1993; Williams et al., 2006). Here atomistic methods allow to study the impact of interstitial elements, mostly without any a-priori assumptions, or to derive required materials data for microscopic theories (such as phase field studies), which cannot be simply measured by experiments.

The present work starts with an overview and classification of different interactions models, beginning with electronic structure theories and ending with empirical atomic potentials. In order to calculate different thermodynamic and thermo-mechanical materials properties we consider in Section 3 and 4 the above mentioned alloy Ag-Cu as well as the corresponding pure components. Two reasons are worth-mentioning for this choice: **(a)** Ag-Cu is of high technical relevance and often employed for high-stressed or high-temperature, brazing connections, e.g. for gas pipe joints. **(b)** According to the high relevance the materials behaviour is well-known and a lot of reference data are available; thus all performed calculations can be easily evaluated. But there is also materials behaviour, which cannot

be directly analyzed by the equations of Sections 3 and 4. In this context mean values and collective behaviour following from the investigation of many particle systems must be considered. One possibility for such an analysis is given by molecular dynamics simulations, which are explained in Section 5. Here we start with a brief description of the basic idea and framework and then exemplarily present simulations subjected to the temporal evolution of a misoriented grain in Titanium at finite temperature. The article ends with concluding remarks and a discussion of future tasks and challenges.

2. Atomic interactions

A central task of atomistic simulation in materials science is to calculate the cohesive energy for a given set of atoms. The many approaches to achieve this goal differ to a great extent in accuracy and computational effort. The common aspect, however, is that the calculated cohesive energy can be utilised to determine a variety of material properties: (i) Differences in the cohesive energies of stable structures are the basis for determining the relative stability of different structures or the formation energy of defects and surfaces. (ii) Differences in the cohesive energy of metastable and unstable structures are required to calculate e.g. the energy barriers for diffusion or phase transformation. (iii) Gradients of the cohesive energy determine the forces acting on the atoms that are needed to carry out structural relaxation or dynamic simulations. (iv) Derivatives of the cohesive energy are required to calculate e.g. elastic properties. In the remainder of this section we describe the approaches that span the regime from highly accurate but computationally expensive electronic-structure calculations to less accurate but computationally cheap empirical interaction potentials.

2.1 Electronic structure theory

One of the most accurate, yet tractable theoretical approaches in materials science is electronic structure theory that we will briefly introduce here. For further information we refer the reader to one of the review papers, e.g. (Bockstedte et al., 1997; Kohn, 1998; Payne et al., 1992), or textbooks, e.g. (Dreizler & Gross, 1990; Parr & Yang, 1989). The starting point of electronic structure theory in materials science is the quantum-mechanical description of the material by the SCHRÖDINGER equation¹

$$(\hat{H} - E)\Psi = (\hat{T}_e + \hat{T}_i + \hat{V}_{e-e} + \hat{V}_{e-i} + \hat{V}_{i-i} - E)\Psi = 0. \quad (1)$$

for ions (i.e. the atomic nuclei) and electrons with a many-body wavefunction Ψ . The terms \hat{V}_{e-e} , \hat{V}_{e-i} and \hat{V}_{i-i} describe the COULOMB interactions between electrons/electrons, electrons/ions, as well as ions/ions. The terms \hat{T}_e and \hat{T}_i denote the kinetic energies of the electrons and ions. The structure and properties of many-body systems can then be determined by solving the SCHRÖDINGER equation. Most practical applications simplify this matter by assuming a decoupled movement of electrons and ions (BORN-OPPENHEIMER approximation (Born & Oppenheimer, 1927)) and thereby reducing the problem to the interaction of the electrons among each other. This interaction is determined by the COULOMB

¹ Without loss of generality we refer through the work to Cartesian coordinates. Scalar quantities are written in italic letters (*s*); vectors are single underlined (*v*); tensors or matrices of second or higher order are double underlined (*T*) or marked by blackboard capital letters (**M**). Operators are indicated by the ($\hat{}$)-symbol. Scalar products between vectors and tensors are marked with (\cdot) or ($\cdot\cdot$), respectively. Greek indices refer to atoms ($\alpha\beta\gamma$) or electrons ($\mu\nu\xi$).

potential and the PAULI principle. There are several approaches to solve the remaining quantum-mechanical problem, the most successful one being density-functional theory that can be considered the today standard method of calculating material properties accurately.

2.2 Density-functional theory

Density-functional theory originates from the KOHN-SHAM formalism (Hohenberg & Kohn, 1964; Kohn & Sham, 1965) that is based on the electron density ρ of a system which describes the number of electrons per unit volume:

$$\rho(\mathbf{r}_1) = N \int \dots \int |\Psi(\mathbf{x}_1, \dots, \mathbf{x}_N)|^2 d\mathbf{x}_2 d\mathbf{x}_N. \quad (2)$$

The volume-integral of this quantity is the total number of electrons

$$\int \rho(\mathbf{r}) d\mathbf{r} = N \quad (3)$$

in the system. KOHN and SHAM mapped the problem of a system of N interacting electrons onto the problem of a set of systems of non-interacting electrons in the effective potential v_{eff} of the other electrons. The SCHRÖDINGER equation for electrons in the non-interacting system is then

$$\left[-\frac{1}{2}\nabla^2 + v_{\text{eff}}(\mathbf{r}) \right] \psi_n(\mathbf{r}) = \varepsilon_n \psi_n(\mathbf{r}), \quad n = 1 \dots N \quad (4)$$

with the electronic density of N electrons of spin s

$$\rho(\mathbf{r}) = \sum_{n=1}^N \sum_s |\psi_n(\mathbf{r}, s)|^2. \quad (5)$$

The effective potential v_{eff}

$$v_{\text{eff}}(\mathbf{r}) = v(\mathbf{r}) + v_{\text{H}}(\mathbf{r}) + v_{\text{xc}}(\mathbf{r}), \quad (6)$$

includes the Hartree-potential v_{H} and the so-called exchange-correlation energy functional $v_{\text{xc}}(\mathbf{r})$ that is not known a priori and that needs to be approximated. The most widely used approximations to the exchange-correlation functional are the *local-density approximation* (LDA) and the *generalized-gradient approximation* (GGA).

2.3 Tight-binding and bond-order potentials

The limitation of DFT to small systems (few 100 atoms) due to the numerical cost can be overcome by taking the description of the electronic structure to an approximate level. This can be carried out rigorously by approximating the density functional theory (DFT) formalism in terms of physically and chemically intuitive contributions within the tight-binding (TB) bond model (Sutton et al., 1988). The TB approximation is sufficiently accurate to predict structural trends as well as sufficiently intuitive for a physically meaningful interpretation of the bonding. The tight-binding model is a coarse-grained description of the electronic structure that expresses the eigenfunctions ψ_n of the KOHN-SHAM equation in a minimal basis

$$\psi_n = \sum_{\alpha\mu} c_{\alpha\mu}^{(n)} \alpha\mu \quad (7)$$

on atoms α with orbitals μ . With an orthonormal basis the solution of the secular equation

$$\sum_{\beta\nu} H_{\alpha\mu\beta\nu} c_{\beta\nu}^{(n)} = E_n c_{\alpha\mu}^{(n)} \quad (8)$$

gives eigenvalues E_n and coefficients $c_{\alpha\mu}^{(n)}$ of the eigenfunctions ψ_n . Here, the elements of the Hamiltonian matrix $\underline{\mathbf{H}}$ are denoted as $H_{\alpha\mu\beta\nu}$. The dependence of these matrix elements from interatomic distance and atomic environment can be parametrised on the basis of DFT calculations. In the tight binding bond model, the binding energy E_B of the system is given as the sum over covalent bond energy E_{bond} , repulsive energy E_{rep} and promotion energy E_{prom}

$$E_B = E_{\text{bond}} + E_{\text{prom}} + E_{\text{rep}} \quad (9)$$

that allows to also include additional contributions from magnetism and charge transfer. The repulsive energy E_{rep} is empirical and often approximated as pairwise term. The change in orbital occupation with respect to the atomic reference state is accounted for by the promotion energy E_{prom} . Both, atom-based information and bond-based information can be used to express the bond energy E_{bond} . These are the so-called onsite and intersite representations that are equivalent but different perspectives of bond formation in materials. The basis of both representations is the set of eigenfunctions ψ_n . The central entity of the atom-based representation is the atomic local density of states (DOS) $n_{\alpha\mu}$ on atom α

$$n_{\alpha\mu}(E) = \sum_n \left| c_{\alpha\mu}^{(n)} \right|^2 \delta(E - E_n) \quad (10)$$

whereas the bond-based representation is footed on the bond-order $\Theta_{\alpha\mu\beta\nu}$ or the density matrix $\rho_{\alpha\mu\beta\nu}$ between orbital μ on atom α and orbital ν on atom β over the occupied states

$$\Theta_{\alpha\mu\beta\nu} = 2\rho_{\alpha\mu\beta\nu} = 2 \sum_n^{\text{occ}} c_{\alpha\mu}^{*(n)} c_{\beta\nu}^{(n)} \quad (11)$$

The bond energy in the equivalent representations is given by

$$E_{\text{bond}} = 2 \sum_{\alpha\mu} \int_{-\infty}^{E_F} (E - E_{\alpha\mu}) n_{\alpha\mu}(E) dE = \sum_{\alpha\mu \neq \beta\nu} \Theta_{\alpha\mu\beta\nu} H_{\alpha\mu\beta\nu} \quad (12)$$

with the FERMI level E_F . The diagonalisation of the HAMILTONIAN matrix $H_{\alpha\mu\beta\nu}$ is the most demanding part of a tight-binding calculation and the limiting factor for its computational efficiency. Compared to DFT, a TB calculation is several orders of magnitude faster and can handle up to a few 10000 atoms.

This limitation can be overcome by bond-order potentials that lead a step further in coarse-graining the description of the electronic structure. Instead of the diagonalisation of the HAMILTON matrix as in the tight-binding problem, the problem is solved locally in terms of the atom-based DOS or the bond-based bond-order. This is computationally more efficient. Moreover, the involved relation of the electronic structure to the local topology and coordination of the material leads to a physically transparent description of local bond formation. Detailed reviews of bond-order potentials for transition metals,

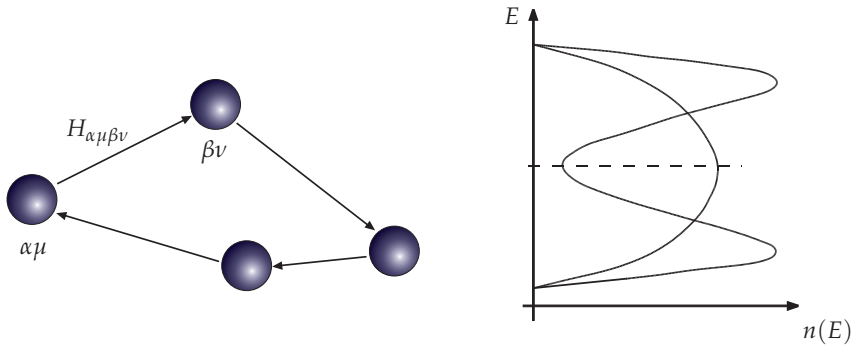


Fig. 3. A self-returning path of length 4 (left) that contributes to the 4-th moment of the DOS (right) on atom i .

semiconductors and hydrocarbons are given elsewhere (Aoki et al., 2007; Drautz et al., 2007; Finnis, 2007a; Mrovec et al., 2007). Some of us recently compiled a more tutorial-like approach to bond-order potentials (Hammerschmidt & Drautz, 2009) and an overview of applications (Hammerschmidt et al., 2009).

A central point in the theory of bond-order potentials is the moments theorem, cf. (Cryot-Lackmann, 1967). It relates the local density of states $n_{\alpha\mu}(E)$ of orbital μ on atom α to products of the HAMILTONIAN matrix elements $H_{\alpha\mu\beta\nu}$:

$$\int E^N n_{\alpha\mu}(E) dE = m_{\alpha\mu}^{(N)} = \sum_{\beta\nu\gamma\xi\ldots} H_{\alpha\mu\beta\nu} H_{\beta\nu\gamma\xi} H_{\gamma\xi\ldots} \cdots H_{\ldots\alpha\mu} \quad (13)$$

This establishes a direct connection between the electronic structure and the local crystal structure. For the N -th moment of atom α , $m_{\alpha}^{(N)}$, the environment is sampled by self-returning paths of length N as illustrated in Figure 3. The higher the moment, the longer the length of the hopping paths and hence the more farsighted the sampling of the atomic environment of atom α . With an infinite number of moments one would recapture the exact solution of the tight-binding problem. The locality of calculating the bond energy is established by terminating the expansion beyond a certain number of moments. This local expansion of the electronic structure using truncated GREEN's function expansion can be carried out in different flavors that are described in detail in, e.g., Refs. (Finnis, 2007b; Horsfield et al., 1996; Pettifor, 1989). The resulting functional form of the bond energy is derived as a function of the atomic positions, where the different ways of integrating the DOS lead to the numerical bond-order potentials (Aoki et al., 2007) and the analytic bond-order potentials for semiconductors (Pettifor & Oleinik, 1999; 2000) and transition metals (Drautz & Pettifor, 2006).

The latter use an expansion of the DOS in terms of CHEBYSHEV polynomials

$$n_{\alpha\mu}(\varepsilon) = \frac{2}{\pi} \sqrt{1 - \varepsilon^2} \left(\sigma_0 + \sum_{n=1} \sigma_n P_n(\varepsilon) \right), \quad (14)$$

where the expansion coefficients σ_n are related to the moments of the DOS by expressing the CHEBYSHEV polynomials explicitly in polynomials with coefficients p_{mk} ,

$$P_m(\varepsilon) = \sum_{k=0}^m p_{mk} \varepsilon^k. \quad (15)$$

This links the expansion coefficients σ_m to the moments $\mu_{i\alpha}^{(k)}$

$$\sigma_m = \sum_{k=0}^m p_{mk} \frac{1}{(2b_{\alpha\infty})^k} \sum_{l=0}^k \binom{k}{l} (-a_{\alpha\infty})^{(k-l)} m_{\alpha\mu}^{(l)}. \quad (16)$$

which leads to a closed-form approximation of the DOS by calculating the moments $m_{\alpha\mu}^{(k)}$ and inserting σ_n into the DOS expansion of Eq. (14).

In this scheme, the integration of the DOS can be carried out analytically and yields an analytic expression for the bond energy, viz.

$$E_{\text{bond},\alpha\mu} = \int_{-E_F}^{E_F} (E - E_{\alpha\mu}) n_{\alpha\mu}(\varepsilon) d\varepsilon = \sum_n \sigma_n [\tilde{\chi}_{n+2}(\phi_F) - \gamma \tilde{\chi}_{n+1}(\phi_F) + \tilde{\chi}_n(\phi_F)]. \quad (17)$$

Here we introduced the so-called response functions

$$\tilde{\chi}_n(\phi_F) = \frac{1}{\pi} \left(\frac{\sin(n+1)\phi_F}{n+1} - \frac{\sin(n-1)\phi_F}{n-1} \right), \quad (18)$$

and the FERMI phase $\phi_F = \cos^{-1}(E_F/2b_{\alpha\infty})$. The bond energy can be taken analytically to an arbitrary number of moments. Therefore the BOPs provide an effective interatomic interaction scheme that converges systematically to the exact solution of the TB HAMILTONIAN. The number of moments required in practice depends on the investigated quantity and is approximately six for identifying qualitative features of structural stability in transition metals (Hammerschmidt et al., 2008) to nine for reproducing quantitative features of defects and transformation paths (Mrovec et al., 2004).

2.4 Empirical potentials

The lowest order approximation of the analytic bond-order potential that includes only two moments is similar to the earlier developed potentials of the FINNIS-SINCLAIR (Finnis & Sinclair, 1984) type or embedded-atom method (EAM) type (Daw & Baskes, 1983; 1984; Foiles et al., 1986). In that sense, the analytic BOP expansion may be viewed as a systematic extension of the FINNIS-SINCLAIR potential to include higher moments. By means of EAM potentials the energy of atom α is expressed as²:

$$E^\alpha = \frac{1}{2} \sum_{\substack{\beta \\ (\alpha \neq \beta)}} \phi^{\alpha\beta}(R^{\alpha\beta}) + F_\alpha(\bar{\rho}_\alpha) \quad \text{with} \quad \bar{\rho}_\alpha = \sum_{\substack{\beta \\ (\alpha \neq \beta)}} \rho_\beta(R^{\alpha\beta}). \quad (19)$$

² The factor $\frac{1}{2}$ appears to avoid double-counting of bonds for $E^{\text{tot}} = \sum E^\alpha$.

The main idea consists of adding a nonlinear function³, F_α , to the pairwise interaction term $\phi^{\alpha\beta}$. This so-called embedding function depends on the electronic density $\bar{\rho}_\alpha$ at the position of atom α , whereas $\phi^{\alpha\beta}$ only depends on the scalar distance $R^{\alpha\beta}$ between atom α and β . In this manner $\bar{\rho}_\alpha$ can be interpreted as a constant background electronic density, that atom α feels due to the superposition of the atomic charge densities ρ_β of its neighbors separated by the distance $R^{\alpha\beta}$. Moreover, F_α can be understood as the energy to put an atom α into a homogeneous electron gas with the density $\bar{\rho}_\alpha$. Here the embedding function itself only depends on the type of the embedded atom and the argument of F_α refers to the medium in which the atom is embedded. Typically the first term of Eq. (19) stands for the purely repulsive ion-ion interaction; the second term characterizes the ion-electron interaction, see also Figure 4. Especially for metals such a decomposition is mostly justified since the valence electrons can nearly free move within the lattice of metallic ions.

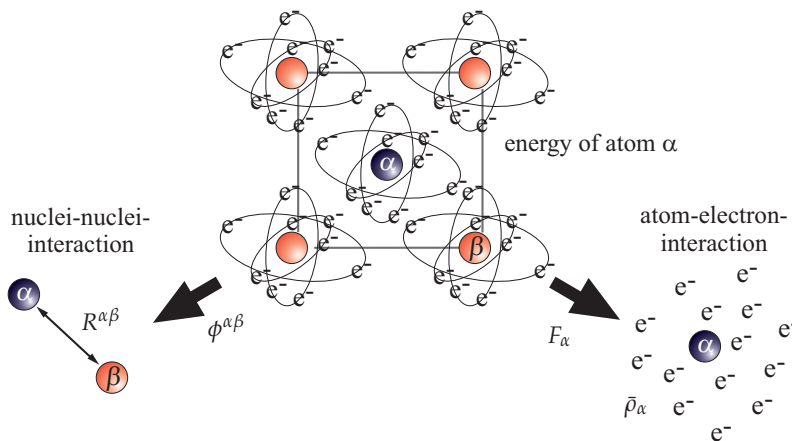


Fig. 4. Illustration of the two contributions to the atom-specific energy according to the EAM framework.

A central aspect of these types of potentials is their tendency to always favor close-packed systems over more open systems due to the purely distant dependent character of interactions. Despite this limitation to purely metallic bonding in fcc/hcp environments, simulations with this class of potentials gave a lot of insight because they are computationally cheap and are routinely applied to very large systems with millions of atoms. The efforts to extend the transferability of these potentials to covalent bonding by introducing additional directional terms (Baskes, 1992) are subsumed as modified embedded-atom methods (MEAM). Complementary approaches that focus on covalently bound structures, semiconductors particularly, are e.g. the potentials of ABELL-TERSOFF (Abell, 1985; Tersoff, 1986) type. Just as the EAM potentials they were defined ad hoc with the goal to stabilise the diamond/zincblende structure over close-packed crystal structures for systems like C, Si, Ge, and GaAs. The functional form of the ABELL-TERSOFF potential is a combination of a repulsive (R) and an

³ The nonlinear character remedies e.g. artifacts like the CAUCHY paradox $C_{1122} = C_{2323}$ or $C_{12} = C_{44}$ (VOIGT notation).

attractive (A) term

$$E^{\alpha} = \sum_{\beta} \left[V_R(R^{\alpha\beta}) - B^{\alpha\beta} V_A(R^{\alpha\beta}) \right] \quad (20)$$

mediated by a term $B^{\alpha\beta}$ that accounts for the local environment in terms of a non-linear dependence on angular terms. Later it turned out, that the particular choice of the angular term in the ABELL-TERSOFF potential has a similar correspondence in bond-order potentials for sp-valent systems (Alinaghian et al., 1993). The ABELL-TERSOFF potentials are slightly more expensive than EAM potentials and can treat similar systems sizes. There are many more empirical potentials available in literature, most notably the LENNARD-JONES potential (Jones, 1924) that is important not only as generic case for algorithm/method development, but also as add-on potential for an empirical description of VAN-DER-WAALS interactions.

For all these empirical potentials, the parametrisation and transferability is a major issue. Many effects of the electronic structure (hybridisation, magnetism, charge transfer) are difficult to be incorporated in the explicit formulation of empirical potentials. The resulting limited transferability gives rise to a dependence of the parametrisation on the considered reference data. Hence the optimal parametrisation for a given element depends often on the envisaged application. This can be partly overcome by giving up a fixed functional form and instead using an interpolating scheme with an open set of functions in the spirit of neural networks (Behler & Parrinello, 2007) or a closed set of functions in the spirit of a reactive force field (van Duin et al., 2001).

2.5 Example: Excess enthalpy of carbon in iron

Several empirical potentials have been proposed for the Fe-C system, due to the great technological relevance for steel production. These models include different parametrisations of the EAM type but also of the MEAM type that incorporates directional bonding. The advantage of using such a comparably simple potential would be the ability to describe microstructural effects that are known to be relevant for fabrication. In the following we will focus on one of the central aspects, the dependence of the solution energy of carbon in α -iron on external volumetric strain. An understanding of this is a prerequisite for predicting the distribution of C within the microstructure of the material. The relation between solubility and strain is also relevant to the interaction of carbon with extended defects such as grain boundaries and dislocations. It can therefore be seen as a critical test to assess if a model of the atomic interactions is applicable to the description of carbon near dislocations.

The solution energy (or excess enthalpy) is calculated by subtracting the cohesive energies of the elemental systems from the cohesive energy of the mixed system at volume V , i.e.

$$\Delta H(V) = E^{\text{FeN}}(V) - E^{\text{FeN}}(V) - E^{\text{C}}(V) \quad (21)$$

where the number of iron atoms N is a variable in the calculations that defines the carbon concentration per unit volume. The calculation of each of these contributions includes a relaxation of the internal degrees of freedom at a fixed volume of the simulation cell.

A recent assessment (Hristova et al., 2011) compared the results of DFT and (M)EAM calculations for the strain-dependent solution energy. These calculations were carried out for a carbon atom in the energetically preferable octahedral interstitial site of a $3 \times 3 \times 3$ unit-cell of α -iron as shown in the left panel of Figure 5. This study showed that DFT calculations

predict a mostly linear decrease of the solution energy with increasing volumetric strain. This

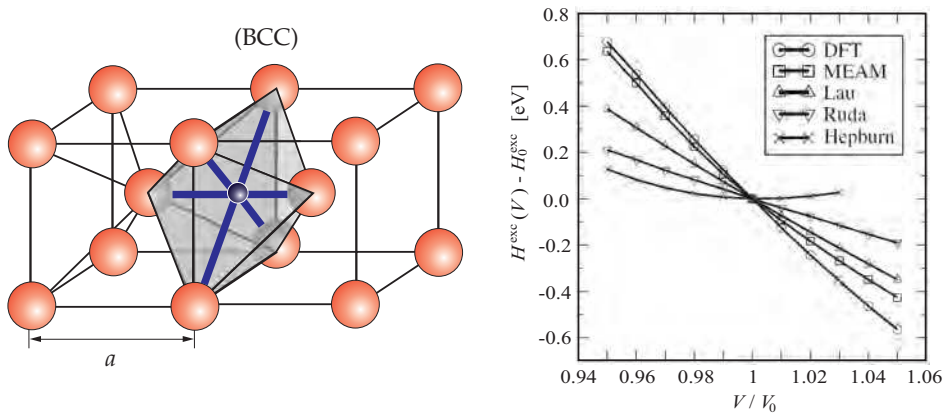


Fig. 5. Calculations of the strain-dependent solubility of C in an octahedral position in α -iron (indicated as the blue atom in left panel) show that only few empirical potentials are able to reproduce the results of corresponding DFT calculations (Hristova et al., 2011) (right panel).

can be understood intuitively in terms of the additional volume of the supercell that can be accommodated by the carbon atom. Despite this comparably simple intuitive picture, the majority of investigated EAM and MEAM potentials deviate noticeably from the DFT results. The overall trend, a decreasing solution energy with increasing strain, is present in all cases. However, the error in the slope ranges from qualitatively wrong to quantitatively reasonable. This example shows the need for developing predictive atomistic models. Once they are available, they can be employed in determining effective material properties as outlined in the next sections.

3. Lattice kinematics and energy

Beyond the task of more or less accurate description of atomic interactions presented in the previous section, the question remains, how to quantify macroscopic materials data and behaviour by considering the energy of an atom. The example in Section 2.5 already indicates the strategy to predict the (un-)mixing behaviour. However, in order to investigate further mechanical and thermodynamic materials properties a "more sophisticated analysis" of the atomic energy is necessary, which will be done in the subsequent Sections.

3.1 Crystal deformations

We start with the consideration of bulk material (no surfaces) and assume a perfect, periodic lattice. The current positions $\underline{\mathbf{X}}^\alpha, \underline{\mathbf{X}}^\beta, \underline{\mathbf{X}}^\gamma, \dots$ of all atoms $\alpha, \beta, \gamma, \dots$ are described by the reference positions $\underline{\mathbf{X}}_0^\alpha, \underline{\mathbf{X}}_0^\beta, \underline{\mathbf{X}}_0^\gamma, \dots$ and the discrete displacements $\underline{\boldsymbol{\zeta}}^\alpha, \underline{\boldsymbol{\zeta}}^\beta, \underline{\boldsymbol{\zeta}}^\gamma, \dots$, namely $\underline{\mathbf{X}}^\alpha = \underline{\mathbf{X}}_0^\alpha + \underline{\boldsymbol{\zeta}}^\alpha, \underline{\mathbf{X}}^\beta = \underline{\mathbf{X}}_0^\beta + \underline{\boldsymbol{\zeta}}^\beta, \dots$ (c.f., Figure 6). By introducing the distance vectors:

$$\underline{\mathbf{R}}_0^{\alpha\beta} = \underline{\mathbf{X}}_0^\beta - \underline{\mathbf{X}}_0^\alpha \quad , \quad \underline{\mathbf{R}}^{\alpha\beta} = \underline{\mathbf{X}}^\beta - \underline{\mathbf{X}}^\alpha = \underline{\mathbf{R}}_0^{\alpha\beta} + \underline{\boldsymbol{\zeta}}^\beta - \underline{\boldsymbol{\zeta}}^\alpha \quad (22)$$

between atom α and β the continuous displacement function $\underline{\mathbf{u}}$ can be defined as follows:

$$\underline{\zeta}^\alpha \equiv \underline{\mathbf{u}}(\underline{\mathbf{X}}_0^\alpha) \equiv \underline{\mathbf{u}}(\underline{\mathbf{X}}_0) \quad , \quad \underline{\zeta}^\beta = \underline{\mathbf{u}}(\underline{\mathbf{X}}_0^\beta) = \underline{\mathbf{u}}(\underline{\mathbf{X}}_0) + \frac{\partial \underline{\mathbf{u}}}{\partial \underline{\mathbf{X}}_0} \cdot \underline{\mathbf{R}}_0^{\alpha\beta} + \dots \quad , \quad (23)$$

$$\underline{\mathbf{R}}^{\alpha\beta} = \underline{\mathbf{R}}_0^{\alpha\beta} + \frac{\partial \underline{\mathbf{u}}}{\partial \underline{\mathbf{X}}_0} \cdot \underline{\mathbf{R}}_0^{\alpha\beta} = \underline{\mathbf{F}} \cdot \underline{\mathbf{R}}_0^{\alpha\beta} \quad . \quad (24)$$

Here the symbol $\underline{\mathbf{F}} = \underline{\mathbf{I}} + \frac{\partial \underline{\mathbf{u}}}{\partial \underline{\mathbf{X}}_0}$ stands for the deformation gradient well known from macroscopic continuum mechanics. In order to describe the potential, temperature-independent energy of a lattice the deformed configuration is expanded into a TAYLOR series around the undeformed lattice state. If terms of higher order would be neglected, the energy of an atom α , $E^\alpha(\underline{\mathbf{R}}^{\alpha 1}, \dots, \underline{\mathbf{R}}^{\alpha N})$, within a deformed lattice consisting of N atoms can be written as:

$$\begin{aligned} E^\alpha(\underline{\mathbf{R}}^{\alpha 1}, \dots, \underline{\mathbf{R}}^{\alpha N}) &= E^\alpha(\underline{\mathbf{R}}_0^{\alpha 1}, \dots, \underline{\mathbf{R}}_0^{\alpha N}) + \sum_{\substack{\beta \\ (\alpha \neq \beta)}} \frac{\partial E^\alpha}{\partial \underline{\mathbf{R}}^{\alpha\beta}} \bigg|_{\underline{\mathbf{R}}_0^{\alpha\beta}} \cdot (\underline{\mathbf{R}}^{\alpha\beta} - \underline{\mathbf{R}}_0^{\alpha\beta}) + \\ &+ \frac{1}{2} \sum_{\substack{\beta \\ (\alpha \neq \beta)}} \frac{\partial^2 E^\alpha}{\partial \underline{\mathbf{R}}^{\alpha\beta} \partial \underline{\mathbf{R}}^{\alpha\beta}} \bigg|_{\underline{\mathbf{R}}_0^{\alpha\beta}} \cdot (\underline{\mathbf{R}}^{\alpha\beta} - \underline{\mathbf{R}}_0^{\alpha\beta}) (\underline{\mathbf{R}}^{\alpha\beta} - \underline{\mathbf{R}}_0^{\alpha\beta}) \quad . \end{aligned} \quad (25)$$

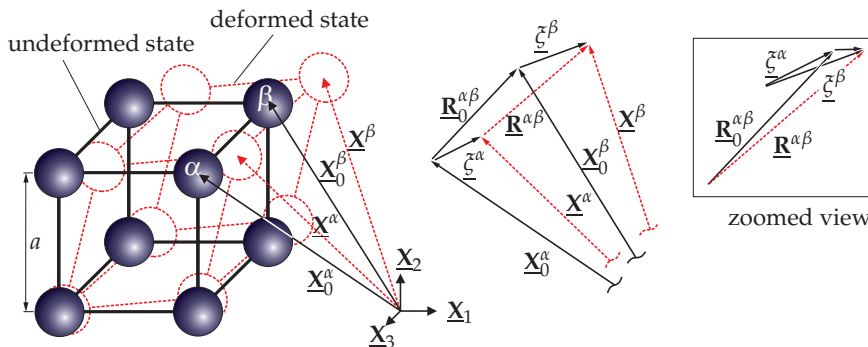


Fig. 6. Kinematic quantities of the undeformed and deformed lattice.

Within standard literature dealing with lattice kinematics, e.g. (Johnson, 1972; 1974; Leibfried, 1955), the linearized strains are introduced by using the approximation $\nabla \underline{\mathbf{u}} \equiv \frac{\partial \underline{\mathbf{u}}}{\partial \underline{\mathbf{X}}_0} \approx \frac{1}{2}(\nabla \underline{\mathbf{u}} + (\nabla \underline{\mathbf{u}})^T) = \underline{\underline{\boldsymbol{\varepsilon}}}$. Substituting $\underline{\mathbf{R}}^{\alpha\beta} - \underline{\mathbf{R}}_0^{\alpha\beta}$ by Eq. (24) yields:

$$\begin{aligned} E^\alpha(\underline{\mathbf{R}}^{\alpha 1}, \dots, \underline{\mathbf{R}}^{\alpha N}) &= E^\alpha(\underline{\mathbf{R}}_0^{\alpha 1}, \dots, \underline{\mathbf{R}}_0^{\alpha N}) + \underline{\underline{\boldsymbol{\varepsilon}}} \cdot \sum_{\substack{\beta \\ (\alpha \neq \beta)}} \frac{\partial E^\alpha}{\partial \underline{\mathbf{R}}^{\alpha\beta}} \bigg|_{\underline{\mathbf{R}}_0^{\alpha\beta}} \underline{\mathbf{R}}_0^{\alpha\beta} + \\ &+ \frac{1}{2} \underline{\underline{\boldsymbol{\varepsilon}}} \cdot \left(\sum_{\substack{\beta \\ (\alpha \neq \beta)}} \underline{\mathbf{R}}_0^{\alpha\beta} \frac{\partial^2 E^\alpha}{\partial \underline{\mathbf{R}}^{\alpha\beta} \partial \underline{\mathbf{R}}^{\alpha\beta}} \bigg|_{\underline{\mathbf{R}}_0^{\alpha\beta}} \underline{\mathbf{R}}_0^{\alpha\beta} \right) \cdot \underline{\underline{\boldsymbol{\varepsilon}}}^T \quad . \end{aligned} \quad (26)$$

An alternative formulation of E^α is given by considering the scalar product of the atomic distance vector $\underline{\mathbf{R}}^{\alpha\beta}$, viz.

$$R^{\alpha\beta 2} = \underline{\mathbf{R}}^{\alpha\beta} \cdot \underline{\mathbf{R}}^{\alpha\beta} = (\underline{\mathbf{F}} \cdot \underline{\mathbf{R}}_0^{\alpha\beta}) \cdot (\underline{\mathbf{F}} \cdot \underline{\mathbf{R}}_0^{\alpha\beta}) = R_0^{\alpha\beta 2} + \underline{\mathbf{R}}_0^{\alpha\beta} \cdot (\underline{\mathbf{C}} - \underline{\mathbf{I}}) \cdot \underline{\mathbf{R}}_0^{\alpha\beta} \quad , \quad (27)$$

in which GREEN's strain tensor $\underline{\mathbf{G}} = \frac{1}{2}(\underline{\mathbf{C}} - \underline{\mathbf{I}})$ with $\underline{\mathbf{C}} = \underline{\mathbf{F}}^T \cdot \underline{\mathbf{F}}$ is used to quantify the deformation (for small deformations holds $\underline{\mathbf{G}} \approx \underline{\mathbf{E}}$). Now the energy of Eq. (26) can be rewritten as follows:

$$\begin{aligned} E^\alpha(R^{\alpha 1^2}, \dots, R^{\alpha N^2}) &= E^\alpha(R_0^{\alpha 1^2}, \dots, R_0^{\alpha N^2}) + 2\underline{\mathbf{G}} \cdot \sum_{\substack{\beta \\ (\alpha \neq \beta)}} E^{\alpha'} \underline{\mathbf{R}}_0^{\alpha\beta} \underline{\mathbf{R}}_0^{\alpha\beta} + \\ &+ \frac{4}{2} \underline{\mathbf{G}} \cdot \left(\sum_{\substack{\beta \\ (\alpha \neq \beta)}} E^{\alpha''} \underline{\mathbf{R}}_0^{\alpha\beta} \underline{\mathbf{R}}_0^{\alpha\beta} \underline{\mathbf{R}}_0^{\alpha\beta} \underline{\mathbf{R}}_0^{\alpha\beta} \right) \cdot \underline{\mathbf{G}} \end{aligned} \quad (28)$$

with the abbreviation $E^{\alpha'} = \partial E^\alpha / \partial R^{\alpha\beta 2} |_{R^{\alpha\beta 2} = R_0^{\alpha\beta 2}}$. Since first derivatives of the energy must vanish for equilibrium (minimum of energy) this expression allows to directly identify the equilibrium condition, which - in turn - provides an equation for calculating the lattice parameter a . Furthermore the last term of Eq. (28) can be linked to the stiffness matrix $\mathbf{C} = [C_{ijkl}]$, which contains the elastic constants of the solid. However, the atomic energy E^α in Eq. (28) must be formulated in terms of the square of the scalar distances $R^{\alpha\beta}$ between the atoms $\alpha, \beta = 1, \dots, N$.

3.2 Brief survey of JOHNSON's analytical embedded-atom method

The specific form of E^α , $E^{\alpha'}$ and $E^{\alpha''}$ in Eq. (28) strongly depends on the chosen interaction model and the corresponding parametrization, i.e., the chosen form of the function(s), which contribute(s) to the potential energy. Therefore we restrict the following explanations to so-called EAM potentials, which were developed in the mid-1980s years by DAW & BASKES and which were successfully applied to a wide range of metals, see also Section 2.4.

In order to quantify the different interaction terms in Eq. (19) parametrizations for $\phi^{\alpha\beta}$, F_α and ρ_β are required. Here JOHNSON (Johnson, 1988; 1989) published an analytical version of the EAM, which incorporates nearest-neighbors-interactions, i.e. atoms only interact with direct neighbors separated by the nearest neighbor distance $R_0 = a^{(e)} / \sqrt{2}$ or $R = a\sqrt{2}$ (in case of an FCC lattice), respectively. Here the symbol a denotes the lattice parameter and the index (e) stands for "equilibrium". By considering the pure substance "A" the following, monotonically decreasing form for the atomic charge density⁴ and the pairwise interaction term holds⁵

$$\rho_A(R^2) = \rho^{(e)} \exp \left[-\beta \left(\frac{R^2}{R_0^2} - 1 \right) \right] \quad , \quad \phi^{AA}(R^2) = \phi^{(e)} \exp \left[-\gamma \left(\frac{R^2}{R_0^2} - 1 \right) \right] \quad . \quad (29)$$

⁴ This form corresponds the spherical s-orbitals; consequently this method mainly holds for isotropic structures, such as FCC (Face-Centered-Cubic), cf. Figure 7. For more anisotropic configurations, such as BCC (Body-Centered-Cubic) or HCP (Hexagonal-Closed-Packed), ρ_α must be varied for different directions, which lead to the Modified-EAM (Bangwei et al., 1999; Baskes, 1992; Zhang et al., 2006).

⁵ For convenience we omit the index "A" at the parameters $\rho^{(e)}$, β , $\phi^{(e)}$, γ and R . The same parametrizations hold for another pure substance "B". However ρ_A and ρ_B as well as ϕ^{AA} and ϕ^{BB} have different fitting parameters.

Originally, JOHNSON used the scalar distance R within the above equations, but due to the explanations in Section 3.1 the present formulation in terms of R^2 is used by simple substitution (Böhme et al., 2007). By using the universal equation of state derived by ROSE and COWORKERS (Rose et al., 1984) the embedding function reads:

$$F_A(\rho_A) = -E_{\text{sub}} \left[1 + \alpha \left(\sqrt{1 - \frac{1}{\beta} \ln \frac{\bar{\rho}_A}{\bar{\rho}_A^{(e)}}} - 1 \right) \right] \exp \left[\alpha \left(1 - \sqrt{1 - \frac{1}{\beta} \ln \frac{\bar{\rho}_A}{\bar{\rho}_A^{(e)}}} \right) \right] - 6\phi^{(e)} \left(\frac{\bar{\rho}_A}{\bar{\rho}_A^{(e)}} \right)^{\frac{\gamma}{\beta}} \quad (30)$$

with $\alpha = \sqrt{\kappa \Omega^{(e)} / E_{\text{sub}}}$; ($\Omega^{(e)}$: volume per atom). Hence three functions ϕ^{AA} , ρ_A , and F_A must be specified for the pure substance "A", which is done by fitting the five parameters $\alpha, \beta, \gamma, \phi^{(e)}, \rho^{(e)}$ to experimental data such as bulk modulus κ , shear modulus G , unrelaxed vacancy formation energy E_V^u , and sublimation energy E_{sub} (Böhme et al., 2007). For mixtures additional interactions must be considered and, therefore, the number of required fit-parameters considerably increases. For a binary alloy "A-B" seven functions $\phi^{AA}, \phi^{BB}, \phi^{AB}, \rho_A, \rho_B, F_A, F_B$ must be determined. Here the pairwise interaction, ϕ^{AB} , between atoms of different type is defined by "averaging" as follows:

$$\phi^{AB} = \frac{1}{2} \left(\frac{\rho_B}{\rho_A} \phi^{AA} + \frac{\rho_A}{\rho_B} \phi^{BB} \right) \quad (31)$$

Consequently all functions are calculated from information of the pure substances; however 10 parameter must be fitted. In Figure 8 the different functions according to Eq. (19) are illustrated for both FCC-metals Ag and Cu. The experimental data used to fit the EAM parameters are shown in Table 1.

atom	a in Å	E_{sub} in eV	E_V^u in eV	κ in eV/Å ³	G in eV/Å ³
Ag	4.09	2.85	1.10	0.65	0.21
Cu	3.61	3.54	1.30	0.86	0.34

Table 1. Experimental data for silver and copper (the volume occupied by a single atom is calculated via $\Omega = a^3/4$).

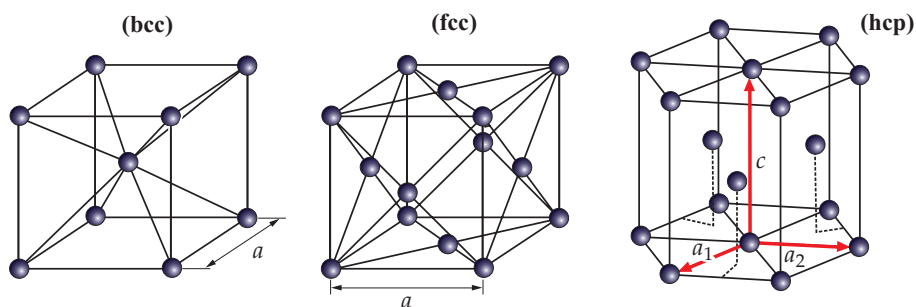


Fig. 7. Elementary cell of the BCC, FCC and HCP lattice.

3.3 Equilibrium condition, elastic constants, and lattice energy

A. Pure substances

By means of Eq. (19) the atomic energy in Eq. (28) can be further specified. For this reason we use the relation $R^{\alpha\beta 2} = R_0^{\alpha\beta 2} + \underline{\mathbf{R}}_0^{\alpha\beta} \cdot \underline{\mathbf{G}} \cdot \underline{\mathbf{R}}_0^{\alpha\beta}$ derived in Section 3.1 and expand $\phi^{\alpha\beta}(R^{\alpha\beta 2}), \rho_\beta(R^{\alpha\beta 2})$ as well as $F_\alpha(\sum \rho_\beta(R^{\alpha\beta 2}))$ around $R_0^{\alpha\beta 2}$. Then the energy of atom α reads:

$$E^\alpha = \frac{1}{2} \sum_\beta \phi^{\alpha\beta}(R_0^{\alpha\beta 2}) + F_\alpha(\bar{\rho}_\alpha^{(e)}) + \underline{\mathbf{G}} \cdot [\underline{\mathbf{A}}^\alpha + 2F'_\alpha(\bar{\rho}_\alpha^{(e)})\underline{\mathbf{V}}^\alpha] + \underline{\mathbf{G}} \cdot [\mathbb{B}^\alpha + 2F'_\alpha(\bar{\rho}_\alpha^{(e)})\mathbb{W}^\alpha + 2F''_\alpha(\bar{\rho}_\alpha^{(e)})\underline{\mathbf{V}}^\alpha \underline{\mathbf{V}}^\alpha] \cdot \underline{\mathbf{G}} \quad (32)$$

in which the following abbreviations hold:

$$\begin{aligned} \underline{\mathbf{A}}^\alpha &= \sum_\beta \phi'^{\alpha\beta}(R_0^{\alpha\beta 2}) \underline{\mathbf{R}}_0^{\alpha\beta} \underline{\mathbf{R}}_0^{\alpha\beta} \\ \mathbb{B}^\alpha &= \sum_\beta \phi''^{\alpha\beta}(R_0^{\alpha\beta 2}) \underline{\mathbf{R}}_0^{\alpha\beta} \underline{\mathbf{R}}_0^{\alpha\beta} \underline{\mathbf{R}}_0^{\alpha\beta} \underline{\mathbf{R}}_0^{\alpha\beta} \quad , \\ \underline{\mathbf{V}}^\alpha &= \sum_\beta \rho'_\beta(R_0^{\alpha\beta 2}) \underline{\mathbf{R}}_0^{\alpha\beta} \underline{\mathbf{R}}_0^{\alpha\beta} \\ \mathbb{W}^\alpha &= \sum_\beta \rho''_\beta(R_0^{\alpha\beta 2}) \underline{\mathbf{R}}_0^{\alpha\beta} \underline{\mathbf{R}}_0^{\alpha\beta} \underline{\mathbf{R}}_0^{\alpha\beta} \underline{\mathbf{R}}_0^{\alpha\beta} \quad . \end{aligned} \quad (33)$$

Note that in case of equilibrium the nearest neighbor distance is equal for all neighbors β , viz. $R_0^{\alpha\beta} = R_0 = \text{const.}$ By considering an FCC lattice with 12 nearest neighbors one finds $\frac{1}{2} \sum_\beta \phi^{\alpha\beta}(R_0^{\alpha\beta 2}) = 6\phi^{(e)}$ and $\bar{\rho}_\alpha^{(e)} = 12\rho_\alpha^{(e)}$.

Three parts of Eq. (33) are worth-mentioning: The first two terms represent the energy of atom α within an undeformed lattice. The term within the brackets [...] of the third summand denotes the slope of the energy curves in Figure 8 (a). If lattice dynamics is neglected, the relation $\underline{\mathbf{A}}^\alpha + 2F'_\alpha(\bar{\rho}_\alpha^{(e)})\underline{\mathbf{V}}^\alpha = 0$ will identify the *equilibrium condition* and defines the nearest neighbor distance in equilibrium. The expression within the brackets $\underline{\mathbf{G}} \cdot [\dots] \cdot \underline{\mathbf{G}}$ of the last term can be linked to the macroscopic constitutive equation $E_{\text{elast}}/V = \frac{1}{2} \underline{\mathbf{E}} \cdot \underline{\mathbf{C}} \cdot \underline{\mathbf{E}}$ with $\underline{\mathbf{G}} \approx \underline{\mathbf{E}}$ (HOOKE's law). Here $\underline{\mathbf{C}}$ stands for the *stiffness matrix* and the coefficients $[C_{ijkl}]$ represent the *elastic constants*. In particular we note: $\underline{\mathbf{C}}^\alpha = \frac{2}{\Omega^{(e)}} [\mathbb{B}^\alpha + 2F'_\alpha(\bar{\rho}_\alpha^{(e)})\mathbb{W}^\alpha + 2F''_\alpha(\bar{\rho}_\alpha^{(e)})\underline{\mathbf{V}}^\alpha \underline{\mathbf{V}}^\alpha]$. Thus, in case of the above analyzed metals Ag and Cu, we obtain the following atomistically calculated values⁶ (for comparison the literature values (Kittel, 1973; Leibfried, 1955) are additionally noted within the parenthesis):

$$\begin{aligned} C_{1111}^{\text{Ag}} &= 132.6 \text{ (124) GPa} \quad , \quad C_{1122}^{\text{Ag}} = 90.2 \text{ (94) GPa} \quad , \quad C_{2323}^{\text{Ag}} = 42.4 \text{ (46) GPa} \quad , \\ C_{1111}^{\text{Cu}} &= 183.7 \text{ (168) GPa} \quad , \quad C_{1122}^{\text{Cu}} = 115.1 \text{ (121) GPa} \quad , \quad C_{2323}^{\text{Cu}} = 68.7 \text{ (75) GPa} \quad , \end{aligned}$$

with $C_{1111} = C_{2222} = C_{3333}$; $C_{1122} = C_{1133} = C_{2233}$; $C_{2323} = C_{1313} = C_{1212}$ and $C_{ijkl} = C_{klij}$. Obviously the discrepancy between the theoretical calculations and experimental findings is

⁶ There are three non-equivalent elastic constants for cubic crystals (Leibfried, 1955).

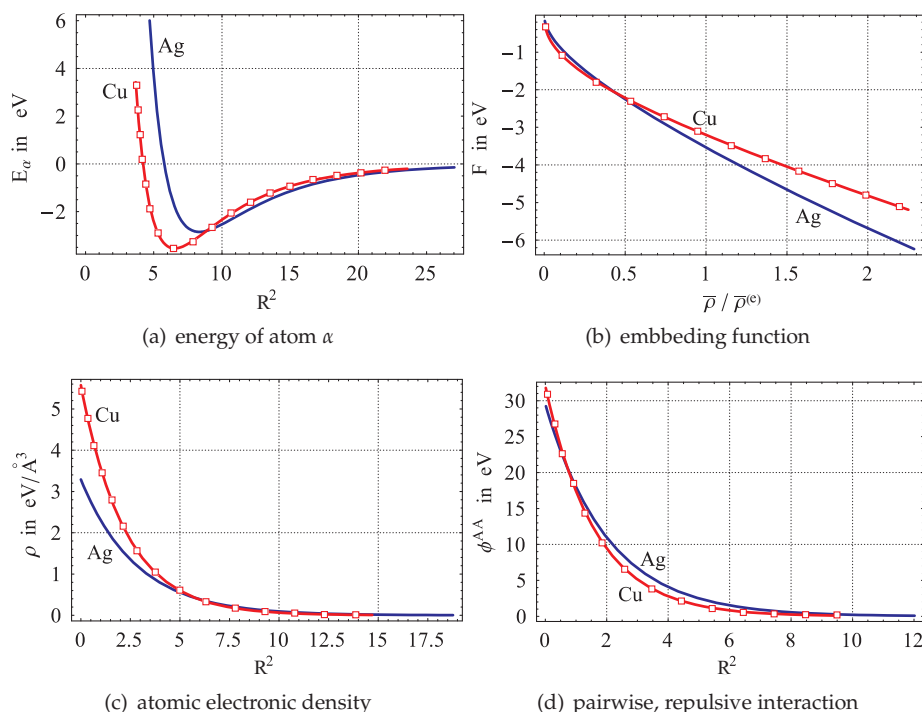


Fig. 8. Different contributions to the EAM potential for silver ($\alpha = 5.92$, $\beta = 2.98$, $\gamma = 4.13$, $\phi^{(e)} = 0.48 \text{ eV}/\text{\AA}^3$, $\rho^{(e)} = 0.17 \text{ eV}/\text{\AA}^3$) and copper ($\alpha = 5.08$, $\beta = 2.92$, $\gamma = 4.00$, $\phi^{(e)} = 0.59 \text{ eV}/\text{\AA}^3$, $\rho^{(e)} = 0.30 \text{ eV}/\text{\AA}^3$).

reasonably good; the relative error range is $4.1 (C_{1111}^{\text{Ag}}) - 9.3 (C_{1111}^{\text{Cu}})$ percent.

B. Alloys

Up to now we only discussed atomic interactions between atoms of the same type. Consequently the question arises, how to exploit the energy expression in Eq. (32) for solid mixtures. To answer this question we have to clarify, how different "types of atoms" can be incorporated within the above set of equations. For this reason let us consider a non-stoichiometric (the occupation of lattice sites by solute substance takes place stochastically, no reactions occur) *binary alloy* "A-B" with the atomic concentration y . Hence we must distinguish the following interactions: $A \Leftrightarrow A$, $B \Leftrightarrow B$, $A \Leftrightarrow B$. Following DE FONTAINE (De Fontaine, 1975) we introduce the discrete concentration $\hat{y}_\gamma = \delta_{\gamma B}$; $\gamma = \{1, \dots, N\}$, where δ_{ij} is the KRONECKER symbol. Then $\phi^{\alpha\beta}$ and $\bar{\rho}_\alpha^{(e)}$ can be written as:

$$\phi^{\alpha\beta} = \phi^{AA} + [\hat{y}_\alpha + (1 - 2\hat{y}_\alpha)\hat{y}_\beta] \phi + (\hat{y}_\alpha + \hat{y}_\beta) \tilde{\phi}, \quad (34)$$

$$\bar{\rho}_\alpha^{(e)} = \sum_\beta [\hat{y}_\beta (\rho_B - \rho_A) + \rho_A] \quad (35)$$

with the definitions $\phi = \phi^{AB} - \frac{1}{2}(\phi^{AA} + \phi^{BB})$ and $\tilde{\phi} = \frac{1}{2}(\phi^{BB} - \phi^{AA})$. Here \hat{y}_γ acts as a "selector", which provides the corresponding interaction terms depending on which pair of atoms is considered. Thus, in particular, $\hat{y}_{\alpha/\beta}$ are both zero, if two "A" atoms are considered and $\phi^{\alpha\beta} = \phi^{AA}$ and $\bar{\rho}_\alpha^{(e)} = \sum_\beta \rho_A$ would follow. Replacing the discrete concentrations by its continuous counterpart:

$$\hat{y}_\alpha = y(\mathbf{X}_0^\alpha) \equiv y(\mathbf{X}_0) \quad , \quad \hat{y}_\beta = y(\mathbf{X}_0) + \frac{\partial y}{\partial \mathbf{X}_0} \cdot \mathbf{R}_0^{\alpha\beta} + \frac{1}{2} \frac{\partial^2 y}{\partial \mathbf{X}^2} \cdot \mathbf{R}_0^{\alpha\beta} \mathbf{R}_0^{\alpha\beta} \quad (36)$$

yields the so-called mean-field limit⁷, viz.

$$\phi^{\alpha\beta} = \phi^{AA} + 2y(1-y)\phi + 2y\tilde{\phi} + \mathcal{O}(\nabla y, \nabla^2 y) \quad , \quad (37)$$

$$\bar{\rho}_\alpha^{(e)} = \bar{\rho}_A + y\bar{\rho}_\Delta + \mathcal{O}(\nabla y, \nabla^2 y) \quad \text{with} \quad \bar{\rho}_\Delta = \sum_\beta (\bar{\rho}_B - \bar{\rho}_A) \quad . \quad (38)$$

In a similar manner the embedding function F_α in Eq. (32) is decomposed:

$$F_\alpha(\bar{\rho}_\alpha^{(e)}) = (1-y)F_A + yF_B \quad , \quad (39)$$

but note that the argument of $F_{A/B}$ is also defined by a decomposition according to Eq. (38). Therefore F_A and F_B are separately expanded into a TAYLOR series around the weighted averaged electron density $\bar{\rho}_{av} = (1-y)\bar{\rho}_A + y\bar{\rho}_B$, namely $F_{A/B}(\bar{\rho}_\alpha^{(e)}) = F_{A/B}(\bar{\rho}_{av}) + \mathcal{O}(\nabla^2 y)$. Moreover, the quantities $\underline{\mathbf{A}}^\alpha$, \mathbb{B}^α , $F'_\alpha \underline{\mathbf{V}}^\alpha$, $F''_\alpha \underline{\mathbf{V}}^\alpha \underline{\mathbf{V}}^\alpha$, and $F'_\alpha \mathbf{W}^\alpha$ can be also treated analogously to Eqs. (39-37). Finally, one obtains for the energy of an atom α within a binary alloy, see also (Böhme et al., 2007) for a detailed derivation:

$$\begin{aligned} E^\alpha(y) = & \frac{1}{2}g^{AA} + F_A + yg^{\tilde{\phi}} + y(F_B - F_A) + y(1-y)g^\phi + \\ & + \underline{\mathbf{G}} \cdot \left[\underline{\mathbf{A}}^A + 2y\underline{\mathbf{A}}^{\tilde{\phi}} + 2y(1-y)\underline{\mathbf{A}}^\phi + 2(\underline{\mathbf{V}}^A + y\underline{\mathbf{V}}^\Delta) \left(F'_A + y(F'_B - F'_A) \right) \right] + \\ & + \frac{1}{2}\underline{\mathbf{G}} \cdot \left[2\mathbb{B}^A + 4y\mathbb{B}^{\tilde{\phi}} + 2y(1-y)\mathbb{B}^\phi + 4(\mathbf{W}^A + y\mathbf{W}^\Delta) \left(F'_A + y(F'_B - F'_A) \right) \right] + \\ & + 4(\underline{\mathbf{V}}^A + y\underline{\mathbf{V}}^\Delta) (\underline{\mathbf{V}}^A + y\underline{\mathbf{V}}^\Delta) \left(F''_A + y(F''_B - F''_A) \right) \Big] \cdot \underline{\mathbf{G}} + \mathcal{O}(\nabla y, \nabla^2 y) \quad (40) \end{aligned}$$

with the abbreviations: $g^{AA} = \sum_\beta \phi^{AA}$, $g^\phi = \sum_\beta \phi$, $g^{\tilde{\phi}} = \sum_\beta \tilde{\phi}$. The remaining abbreviations $\underline{\mathbf{A}}^A$, $\underline{\mathbf{A}}^\phi$, $\underline{\mathbf{A}}^{\tilde{\phi}}$, \mathbb{B}^ϕ , $\mathbb{B}^{\tilde{\phi}}$, $\underline{\mathbf{V}}^\Delta$, and \mathbf{W}^Δ are defined correspondingly to Eq. (33); here the indices A, ϕ , $\tilde{\phi}$, and Δ refer to the first argument within the sum, i.e. $\phi^{AA'}$; ϕ' or ϕ'' ; $\tilde{\phi}'$ or $\tilde{\phi}''$, and $(\rho'_B - \rho'_A)$ or $(\rho''_B - \rho''_A)$. Eq. (40) indicates various important conclusions:

- The terms of the **first row** stand for the energy of the undeformed lattice. Here no mechanical effects contributes to the energy of the (homogeneous) solid. These energy

⁷ For homogeneous mixtures concentration gradients can be neglected; for mixtures with spatially varying composition terms with $\nabla y = \partial y / \partial \mathbf{X}_0$ and $\nabla^2 y = \partial^2 y / \partial \mathbf{X}_0^2$ contribute e.g. to phase kinetics, cf. (Böhme et al., 2007).

terms are typically used in equilibrium thermodynamics to determine GIBBS free energy and phase diagrams.

- The **second row**, in particular the expression within the brackets [...], identifies the *equilibrium condition* since first derivatives of the energy must vanish in equilibrium. Analyzing the root

$$\underline{\underline{A}}^A + 2y\underline{\underline{A}}^{\tilde{\phi}} + 2y(1-y)\underline{\underline{A}}^{\phi} + 2(\underline{\underline{V}}^A + y\underline{\underline{V}}^{\Delta})\left(F'_A + y(F'_B - F'_A)\right) \equiv 0 \quad (41)$$

yields $a^{(e)}(y)$ as a function of the concentration, cf. example below.

- The term of the **third and last row** denotes the elastic energy $E^{\text{elast}} = \frac{1}{2}\underline{\underline{\mathcal{E}}} \cdot \underline{\underline{C}}(y) \cdot \underline{\underline{\mathcal{E}}}$ with $\underline{\underline{\mathcal{E}}} \approx \underline{\underline{G}}$ of an atom in the lattice system. Consequently, the bracket term characterizes the *stiffness matrix* of the solid mixture, viz.

$$\underline{\underline{C}}(y) = \frac{1}{\Omega^{(e)}(y)} \left[2B^A + 4yB^{\tilde{\phi}} + 2y(1-y)B^{\phi} + 4(W^A + yW^{\Delta})\left(F'_A + y(F'_B - F'_A)\right) + \right. \\ \left. + 4(\underline{\underline{V}}^A + y\underline{\underline{V}}^{\Delta})(\underline{\underline{V}}^A + y\underline{\underline{V}}^{\Delta})\left(F''_A + y(F''_B - F''_A)\right) \right]. \quad (42)$$

Note that $\Omega^{(e)}(y)$ is calculated by $a^{(e)}(y)$ following from Eq. (41).

Figure 9 (left) displays the left hand side of Eq. (41) as a function of R^2 for different concentrations $y = y_{\text{Cu}}$ in Ag-Cu. The root defines the equilibrium lattice parameter, which is illustrated in Figure 9 (right). Obviously, $a^{(e)}(y)$ does not follow VEGARD's law. However, by using the mass concentration $c(y) = yM_{\text{Cu}} / (yM_{\text{Cu}} + (1-y)M_{\text{Ag}})$ instead of y the linear interpolation $a^{(e)}(c) = (1-c)a_{\text{Ag}} + ca_{\text{Cu}}$ holds.

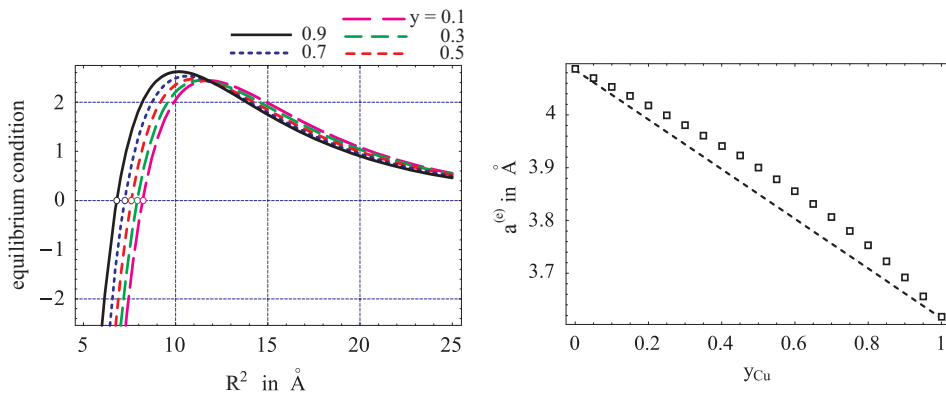


Fig. 9. *Left*: Left hand side of the equilibrium condition for different, exemplarily chosen concentrations ($R_{0,\text{Ag}}^2 = 8.35$, $R_{0,\text{Cu}}^2 = 6.53$). *Right*: Calculated equilibrium lattice parameter as a function of concentration.

The three independent elastic constants for the mixture Ag-Cu are calculated by Eq. (42) and illustrated in Figure 10. Here we used $a^{(e)}(y_i)$, with $y_i = 0, 0.05, \dots, 0.95, 1$ correspondingly to Figure 9 (right). It is easy to see, that for $y = 0$ (Ag) and $y = 1$ (Cu) the elastic constants of

silver and copper, illustrated on page 15, result. However, for $0 < y < 1$ the elements of the stiffness matrix do not follow the linear interpolation as indicated in Figure 10.

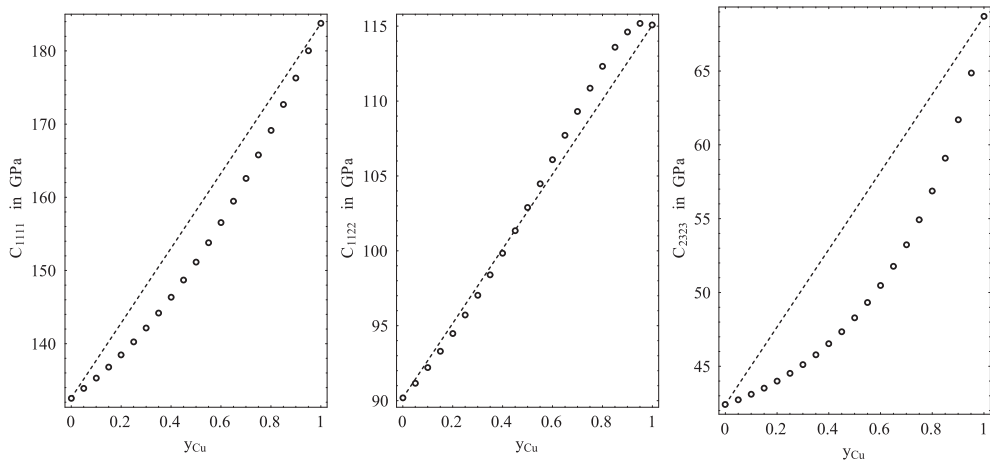


Fig. 10. Calculated elastic constants for Ag-Cu as function of concentration.

Finally, Eq. (40) allows to analyze the so-called *excess enthalpy* g^{exc} of the solid system, which characterizes the (positive or negative) heat of mixing. It represents the deviation of the resulting energy of mixture with concentration y from the linear interpolation of the pure-substance-contributions, cf. Section 2.5. By considering the so-called regular solution model introduced by HILDEBRANDT in 1929, see for example the textbook of (Stølen & Grande, 2003):

$$g^{\text{exc}} = \Lambda y(1 - y) \quad \text{with} \quad y = y_B, \quad y_A = 1 - y \quad (\text{binary alloys}). \quad (43)$$

the excess term can be directly identified in Eq. (40) as the coefficient of $y(1 - y)$. However, the above regular solution model only allows symmetric curves $g^{\text{exc}}(y)$, with the maximum at $y = 0.5$. This shortcoming originates from the constant Λ -value and is remedied within the above energy expression of Eq. (40). In particular holds:

$$\Lambda = \Lambda(y) = g^{\phi}(y) + \underline{\underline{\mathbf{G}}}(y) \cdot \cdot \mathbb{B}^{\phi} \cdot \cdot \underline{\underline{\mathbf{G}}}. \quad (44)$$

Here g^{ϕ} as well as \mathbb{B}^{ϕ} are given by the interatomic potentials⁸ and must be evaluated at the concentration dependent nearest neighbor distance $R_0(y) = a^{(e)}(y)/\sqrt{2}$, which - in turn - follows from the equilibrium condition. Thus, symmetry of Eq. (43) does not necessarily exist. Moreover, further investigations of Eq. (44) may allow a deeper understanding of non-ideal energy-contributions to solid (and mechanically stressed) mixtures.

⁸ Note, that Λ exclusively depends on the pairwise interaction terms; contributions from the embedding functions naturally cancel.

4. Thermodynamic properties

Atomistic approaches for calculating interaction energies cannot only be used to quantify deformation and mechanical equilibrium but may also serve as the basis for accessing thermodynamic and thermo-mechanical properties as we will show in the following section.

4.1 Phase diagram construction

In macroscopic thermodynamics the molar GIBBS free energy of an undeformed binary mixture is typically written as (pressure $P = \text{const.}$):

$$\tilde{g}(y, T) = (1 - y_B)\tilde{g}_A(T) + y_B\tilde{g}_B(T) + N_A k_B T \left[y_B \ln y_B + (1 - y_B) \ln(1 - y_B) \right] + \tilde{g}^{\text{exc}}(y, T). \quad (45)$$

The first and second term represent the contributions from the pure substances; the third summand denotes the entropic part of an ideal mixture $-T\tilde{s}(y) = -N_A k_B T \sum_{i=1}^2 y_i \ln y_i$ with $N_A = 6.022 \cdot 10^{23} \text{ mol}^{-1}$ (AVOGADRO constant) and $k_B = 1.38 \cdot 10^{-23} \text{ J/K}$ (BOLTZMANN constant) and the last term stands for the molar excess enthalpy.

By using the identity $\tilde{g}(y, T) = N_A g(y, T) = N_A [E^{\alpha} - T\tilde{s}(y)]$ the atom-specific GIBBS free energy can be directly calculated from the expression in Eq. (40), viz.

$$g(y, T) = (1 - y_B)(6\phi^{\text{AA}} + F_A) + y(6\phi^{\text{BB}} + F_B) + k_B T \left[y_B \ln y_B + (1 - y_B) \ln(1 - y_B) \right] + 12y(1 - y)\phi. \quad (46)$$

Obviously, the GIBBS free energy curve is superposed by three, characteristic parts, namely **(a)** a linear function interpolating the energy of the pure substances; **(b)** a convex, symmetric entropic part, which has the minimum at $y = 0.5$ and vanishes for $y = \{0, 1\}$ and **(c)** an excess term, which - in case of binary solids with miscibility gap - has a positive, concave curve shape, cf. Figure 11 (right). Hence, a double-well function results, as illustrated in Figure 11 (left) for the cases of Ag-Cu at 1000 K. Here the concave domain $y \in [0.19, 0.79]$ identifies the unstable regime, in which any homogeneous mixture starts to decompose into two different equilibrium phases (α) and (β) with the concentrations $y_{(\alpha)}$, $y_{(\beta)}$, cf. (Cahn, 1968).

In order to determine the equilibrium concentrations the so-called *common tangent rule* must be applied. According to this rule the mixture decomposes such, that the slope of the energy curve at $y_{(\alpha)/\beta}$ is equal to the slope of the connecting line through these points, as illustrated in Figure 11 (left), i.e.

$$\left. \frac{\partial g(y, T)}{\partial y} \right|_{y=y_{(\alpha)}} = \left. \frac{\partial g(y, T)}{\partial y} \right|_{y=y_{(\beta)}} = \frac{g(y_{(\beta)}, T) - g(y_{(\alpha)}, T)}{y_{(\beta)} - y_{(\alpha)}}. \quad (47)$$

Eq. (47) provides two equations for the two unknown variables $y_{(\alpha)/\beta}$. The quantity $g(y, T)$ as well as its derivatives can be directly calculated from the atomistic energy expression in Eq. (46).

Figure 12 (squared points) displays the calculated equilibrium concentrations for different temperatures. Here the dashed lines represent experimental data adopted from the database MTDataTM. As one can easily see, there is good agreement between the experimental

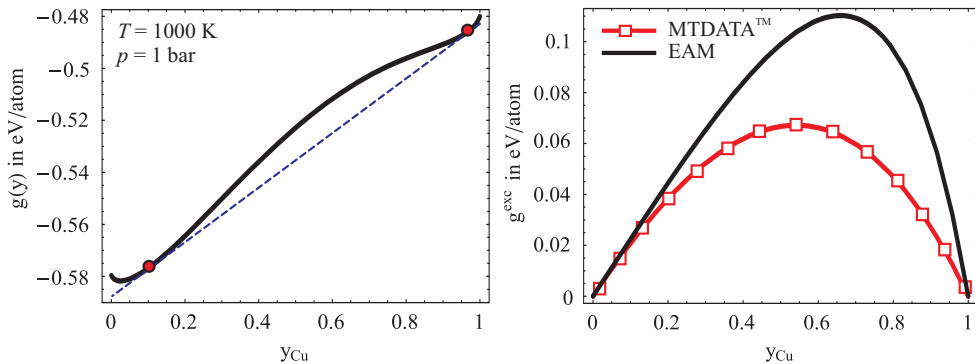


Fig. 11. *Left*: Atomic GIBBS free energy curve for Ag-Cu at 1000 K, adopted from the program package MTDATATM (MTDATA, 1998) including the common tangent (dashed line) for defining the equilibrium concentration. *Right*: Comparison of the theoretically and experimentally obtained atomic excess enthalpy.

and theoretical results. Deviations mainly occur for the high temperature regime and - in particular - for the (β)-phase. Two reasons are worth-mentioning:

- The temperature only enters via the entropic part in Eq. (46); lattice dynamics are neglected up to now. Adding a vibrational term to the energy expression yields an explicitly temperature-depending equilibrium condition and lattice parameter $a^{(e)}(T, y)$, which increases the agreement between experiment and atomistic model, cf. (Najababadi et al, 1993; Williams et al., 2006).
- As indicated in Figure 11 (right) the excess enthalpy crucially determines the concave area of the g -curve and, therefore, $y_{(\alpha)}/y_{(\beta)}$. Obviously, the applied, analytical nearest-neighbor EAM model, cf. Section 3.2, leads to overestimated excess data, as illustrated in Figure 11 (right). Here better results can be found by incorporating more neighbors or increased interaction models, such as MEAM potentials (Feraoun et al., 2001).

However, the calculated solid part of the phase diagram qualitatively and also in a wide range quantitatively reproduces the experimental values and confirms the applicability of the present model for thermodynamic calculations.

4.2 Lattice vibrations, heat capacity, and thermal expansion

Up to now no contributions to the energy resulting from lattice dynamics are considered. Indeed, temperature and (mean) velocity of the particle system are directly coupled and, thus, temperature-depending materials properties can only be precisely determined on the atomistic scale by incorporating lattice vibrations, i.e. phonons.

To this end the lattice is modelled as a 3D-many-body-system, consisting of mass points (atoms) and springs (characterized by interatomic forces). Thus, the equation of motion of atom α can easily be found by the framework of classical mechanics. By considering $m_{\alpha}\ddot{\underline{x}}_{\alpha} = \underline{F}_{\alpha} = -\nabla E^{\alpha}$ and Eq. (25) one can write the following equation of motion for the

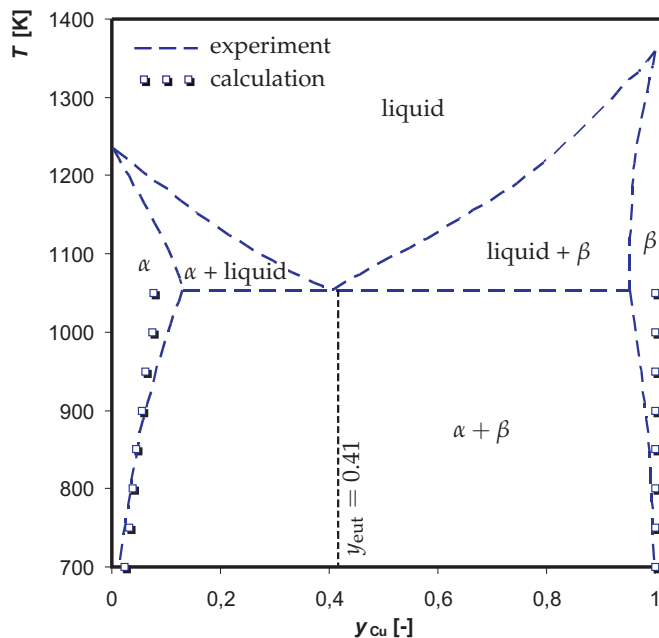


Fig. 12. On the phase diagram construction. Atomistically calculated data (squared points) vs. experimental data (dashed line), adopted from MTDATATM, (MTDATA, 1998).

discrete displacement $\underline{\xi}_\alpha$ of atom α :

$$m_\alpha \ddot{\underline{\xi}}_\alpha = - \sum_\beta \frac{\partial^2 E^\alpha}{\partial \underline{\mathbf{R}}^{\alpha\beta} \partial \underline{\mathbf{R}}^{\alpha\beta}} \bigg|_{\underline{\mathbf{R}}_0^{\alpha\beta}} \cdot (\underline{\mathbf{R}}^{\alpha\beta} - \underline{\mathbf{R}}_0^{\alpha\beta}). \quad (48)$$

In what follows we restrict ourselves to the so-called harmonic approximation, which means that terms beyond quadratic order are neglected in Eq. (25). Please note the identity $\underline{\mathbf{R}}^{\alpha\beta} - \underline{\mathbf{R}}_0^{\alpha\beta} = \underline{\xi}^\beta - \underline{\xi}^\alpha$; consequently Eq. (48) represents a partial differential equation for $\underline{\xi}^\alpha$, which can be solved by the ansatz for planar waves, (Leibfried, 1955):

$$\underline{\xi}^\alpha = \underline{\mathbf{e}} e^{i(\underline{\mathbf{k}} \cdot \underline{\mathbf{X}}_0^\alpha - \omega t)} \quad \text{and} \quad \underline{\xi}^\beta = \underline{\mathbf{e}} e^{i(\underline{\mathbf{k}} \cdot \underline{\mathbf{X}}_0^\beta - \omega t)}. \quad (49)$$

Here $\underline{\mathbf{e}}$ stands for the normalized vector parallel to the direction of the corresponding displacement. Inserting the above ansatz into Eq. (48) yields:

$$m_\alpha \omega^2 \underline{\mathbf{e}} = \sum_\beta \frac{\partial^2 E^\alpha}{\partial \underline{\mathbf{R}}^{\alpha\beta} \partial \underline{\mathbf{R}}^{\alpha\beta}} \bigg|_{\underline{\mathbf{R}}_0^{\alpha\beta}} \cdot \underline{\mathbf{e}} \left(1 - e^{i\underline{\mathbf{k}} \cdot \underline{\mathbf{R}}_0^{\alpha\beta}} \right) = \sum_\beta \underline{\underline{\mathbf{D}}}^{\alpha\beta} (\underline{\mathbf{R}}_0^{\alpha\beta}) \cdot \underline{\mathbf{e}} \left(1 - e^{i\underline{\mathbf{k}} \cdot \underline{\mathbf{R}}_0^{\alpha\beta}} \right). \quad (50)$$

The symbol $\underline{\underline{\mathbf{D}}}^{\alpha\beta}$ represents the force constant matrix, the 3D-analogue to the spring constant within HOOKE's law in one dimension. By combining $\underline{\underline{\mathbf{D}}}^{\alpha\beta}$ and the exponential function yields

the dynamical matrix $\underline{\underline{D}}^{\alpha\beta}(\mathbf{k})$, which can be directly linked to the FOURIER transform of the force constant matrix.

In case of EAM potentials E^α only depends on the distance $R^{\alpha\beta}$ or $R^{\alpha\beta 2}$, respectively. Therefore the chain rule $\partial^2 E^\alpha / (\partial \mathbf{R}^{\alpha\beta})^2 = (\partial^2 E^\alpha / \partial x^2)(\partial x / \partial \mathbf{R}^{\alpha\beta})^2 + (\partial E^\alpha / \partial x)(\partial^2 x / \partial \mathbf{R}^{\alpha\beta 2})$ must be applied to obtain $\underline{\underline{D}}^{\alpha\beta}$.

Furthermore, ω denotes the angular velocity defining the time $\Theta = 2\pi/\omega$ required for one period of the propagating wave; \mathbf{k} identifies the wave vector, which defines the direction of wave propagation and the wave length $\lambda = 2\pi/|\mathbf{k}|$.

Equation (50) represents an eigenvalue problem, which can be solved by the following equation:

$$\det \left[\underbrace{\sum_{\beta} \underline{\underline{D}}^{\alpha\beta}(\mathbf{R}_0^{\alpha\beta}) \left(1 - e^{i\mathbf{k} \cdot \mathbf{R}_0^{\alpha\beta}} \right)}_{=\underline{\underline{D}}^{\alpha\beta}} - \underline{\underline{I}} m_\alpha \omega^2 \right] = 0. \quad (51)$$

The three eigenvalues, $\hat{D}_{I/II/III}(\mathbf{k}) = m_\alpha \omega_{I/II/III}^2(\mathbf{k})$, of the 3×3 matrix $\underline{\underline{D}}^{\alpha\beta}$ yield the eigenfrequencies $\nu_{I/II/III}(\mathbf{k}) = \omega_{I/II/III}(\mathbf{k})/(2\pi)$. Additionally, Eq. (51) defines three eigenvectors $\mathbf{e}^{I/II/III}$ with $\mathbf{e}^k \mathbf{e}^l = \underline{\underline{I}}$ and $k, l \in \{I, II, III\}$, i.e. they form an orthonormal basis. Moreover, $\mathbf{e}^{I/II/III}$ determine the polarization of the wave - namely the oscillation direction of atoms. In particular, one longitudinal wave ($\mathbf{e}^k \parallel \mathbf{k}$) and two transversal waves ($\mathbf{e}^k \perp \mathbf{k}$) can be typically found in an elemental system.

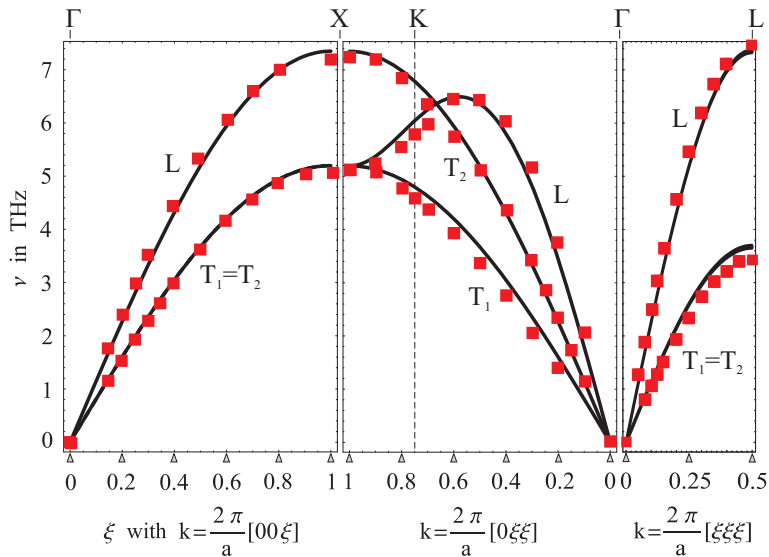


Fig. 13. Phonon dispersion of copper calculated for the three elementary FCC-symmetry directions [001], [011], and [111] with Johnson's nearest neighbor EAM potentials, (Johnson, 1989). Squared, red points identify experimental data at room temperature according to the literature, (Bian et al., 2008; Svensson et al., 1967).

At finite temperature real crystal vibrations show a wide range of wave vectors and frequencies. To quantify the dynamical characteristics of the lattice phonon dispersion curves are measured (or calculated), which displays all frequencies for the lattice-specific symmetry directions. Figure 13 illustrates the phonon dispersion curves, calculated from the atomistic model for copper. Here we considered the three elemental symmetry directions of the FCC-structure, namely $\xi[100]$, $\xi[011]$, and $\xi[111]$ with $\xi \in [0, 2\pi/a^{(e)}]$ or $\xi \in [0, \pi/a^{(e)}]$, respectively (1st BRILLOUIN zone⁹). The squared, discrete points are added for comparative purposes and identify experimental data obtained from (Bian et al., 2008; Svensson et al., 1967).

By means of quantum-mechanics and statistical physics the kinetic energy, resulting from lattice vibrations, can be written as, cf. (Leibfried, 1955):

$$E_{\text{kin}}^{\alpha}(T) = \frac{1}{N} \sum_{i=1}^{3N} \sum_{\mathbf{k}} \frac{h \nu_i(\mathbf{k})}{2} + \frac{1}{N} \sum_{i=1}^{3N} \sum_{\mathbf{k}} \frac{h \nu_i(\mathbf{k})}{\exp\left[\frac{h \nu_i(\mathbf{k})}{k_B T}\right] - 1} \quad , \quad (52)$$

in which the variable $h = 6.626 \cdot 10^{-34}$ Js denotes PLANCK'S constant. Furthermore the summation is performed over all occurring eigenfrequencies ν_1, \dots, ν_{3N} of the N atoms within the lattice system and the wave vectors \mathbf{k} . The relation of Eq. (52) results from considering the $6N$ -dimensional phase space, well-established in statistical mechanics, and by adding the energy-contribution of each oscillator to the partition function Z . Consequently an expression for the total kinetic energy $E_{\text{kin}}^{\text{tot}}$ is obtained, from which E_{kin}^{α} follows by introducing the factor $1/N$. The total energy of atom α can now be written as:

$$E_{\text{tot}}^{\alpha}(T, y) = E_{\text{(EAM)}}^{\alpha}(y) + E_{\text{kin}}^{\alpha}(T) \quad , \quad (53)$$

At this point it is worth-mentioning, that the question of which and how many frequencies ν_i and wave vectors \mathbf{k} are used to quantify $E_{\text{kin}}^{\text{tot}}$ may strongly determine the accuracy of all subsequently derived quantities. In (Bian et al., 2008) the authors, for example, uniformly discretized the BRILLOUIN zone by 20^3 grid points and used a weighted sum of 256 different wave vectors. However, such procedure requires considerable computational capacities since the eigenvalue-problem of Eq. (51) must be solved for each choice of \mathbf{k} . In the present work we exclusively investigated a weighted sum of the eigenfrequencies of the three elemental symmetry directions $[001]$, $[011]$, and $[111]$.

Equation (53) can be interpreted as the relation for the particle-specific internal energy of the solid, in which the temperature is included via the kinetic term. The heat capacity c_v at constant volume¹⁰ can now be calculated by means of the partial derivative:

$$c_v(T, y) = \frac{\partial E_{\text{tot}}^{\alpha}(T, y)}{\partial T} = \frac{dE_{\text{kin}}^{\alpha}(T)}{dT} \quad . \quad (54)$$

Figure 14 compares the calculated heat capacity for copper with the experimental one constructed from the measured EINSTEIN frequency and the homonymous ansatz for c_v , (Fornasini et al., 2004).

⁹ The first BRILLOUIN zone represents the unit cell in the reciprocal lattice, for more details see for example (Yu & Cardona, 2010).

¹⁰ This condition can be guaranteed by setting e.g. $a = a^{(e)}$ but any volume-preserving deformation is possible.

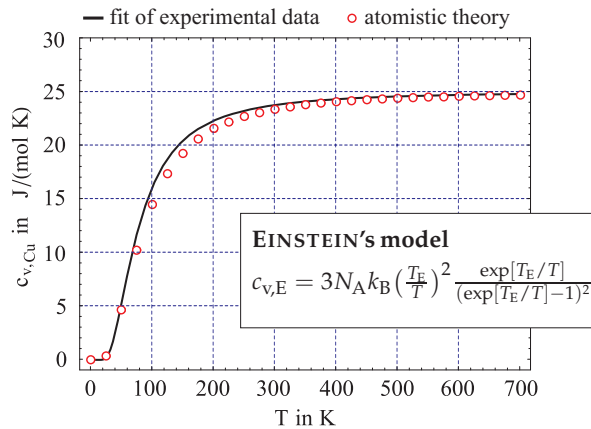


Fig. 14. Molar heat capacity c_v at constant volume, calculated from EAM potentials. The solid line denotes the fitting curve, according to EINSTEIN's model by using the EINSTEIN frequency $\nu_E = T_E k_B / h = 4.96$ THz measured by Extended X-ray-Absorption Fine-Structure (EXAFS), (Fornasini et al., 2004).

Due to the vibrational part the total energy of atom α additionally depends on T . The thermal expansion coefficient can be calculated by expanding E_{tot}^α into a TAYLOR series according to Eqs. (26,28), but additionally incorporating derivatives of T . A subsequent exploitation of terms of mixed derivatives yields the thermal expansion coefficient, cf. (Leibfried, 1955), pp. 235 ff..

An alternative approach for the determination of the thermal expansion coefficient is given by the following illustrative arguments, see also Figure 15 (upper left). For $T = 0$ atom α is situated in the potential energy minimum defined by the equilibrium nearest neighbor distance R_0 . For $T > 0$ the atoms oscillates around the equilibrium position. Here the sum $E_{\text{pot}} + E_{\text{kin}}$ defines the oscillating distance R_- and R_+ , cf. Figure 15 (upper left). The center position $R_{01} = R_- + 0.5(R_+ - R_-)$ defines the equilibrium distance for $T > 0$. Note that R_{01} is greater than R_0 , due to the asymmetry of the energy curve w.r.t. the energy minimum. For increasing temperatures the kinetic energy and R_{01} increase, cf. 15 (upper right), which characterizes the thermal expansion.

Figure 15 (lower left) illustrates the oscillation range $(R_+ - R_-)$ following from both intersections of $E^*(T, R)$ with the horizontal axis and the construction of R_{01} for different temperatures. The resulting nearest neighbor distances are displayed in the lower right panel. By assuming isotropy on the macroscopic level the following equations hold for thermal expansion:

$$\underline{\underline{\epsilon}}^{\text{th}} = \underline{\underline{\alpha}}^{\text{th}}(T)(T - T_{\text{ref}}) \quad , \quad \underline{\underline{\alpha}}^{\text{th}}(T) = \alpha^{\text{th}}(T) \underline{\underline{I}} \quad , \quad \alpha^{\text{th}}(T) = \frac{1}{R_{01}(T)} \frac{dR_{01}(T)}{dT} . \quad (55)$$

An exploitation of Eq. (55) at $T = 300$ K yields the thermal expansion coefficient of $\alpha^{\text{th}} = 9.1 \cdot 10^{-6} \text{ K}^{-1}$. This value is smaller than the corresponding literature value $\alpha_{\text{Cu}}^{\text{th}} \approx 15 \cdot 10^{-6} \text{ K}^{-1}$ (Bian et al., 2008), whereas the temperature dependence $R_{01} = R_{01}(T) \Leftrightarrow a^{(e)} = a^{(e)}(T)$ qualitatively agrees with experimental observations.

The reasons for the deviations are different. First, no anharmonic terms or electronic contributions are considered. Therefore, deviations occur, particularly in the high temperature regime, (Kagaya et al., 1988; Wallace, 1965). Second, the limited consideration of exclusively nine eigenfrequencies according to the three elementary symmetry directions lead to a reduced description of the vibrational energy. Consequently, α^{th} is insufficiently reproduced. Indeed, incorporating more wave vectors leads to more accurate results (Bian et al., 2008; Kagaya et al., 1988), but the computational costs drastically increase.

In case of cubic lattice symmetry the heat capacity at constant pressure, c_p , can be easily calculated via the relation $c_p(T) = c_v(T) + 3T(C_{1111} + 2C_{1122})\alpha_{\text{th}}^2(T)$. Finally we emphasize, that the above framework can be also applied to solid mixtures. For this reason the dynamical matrix $\tilde{\mathbf{D}}^{\alpha\beta}(\mathbf{k}, y)$ must be calculated by the first line of the energy expression in Eq. (40). Please note the additional argument y in $\tilde{\mathbf{D}}^{\alpha\beta}$, and consequently in $v_i(\mathbf{k}, y)$ and $E_{\text{kin}}^{\alpha}(T, y)$. Furthermore one needs the mean field relation $m_{\alpha}(y) = ym_B + (1 - y)m_A$ with $y = y_B$.

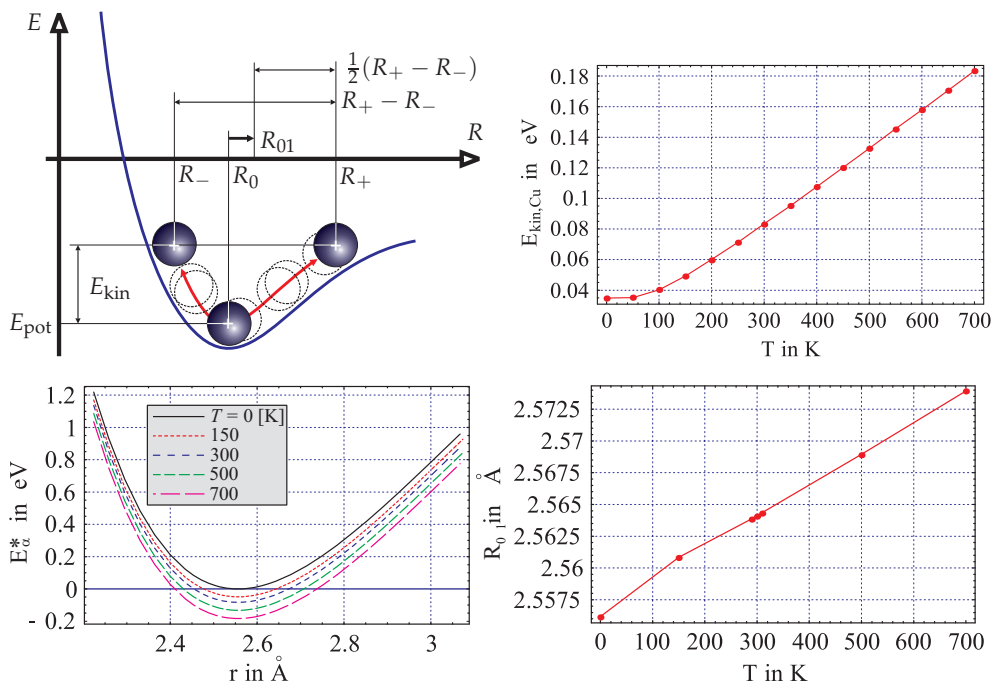


Fig. 15. *Upper left*: On the origin of thermal expansion. The shift from $R_0^{\alpha\beta}$ to $R_{01}^{\alpha\beta}$ results from the asymmetric energy curve around the minimum. *Upper right*: kinetic energy of Cu-atoms calculated for different temperatures. *Lower left*: $E^*(R, T) = E_{\text{pot}}^{\alpha}(R) + [E_{\text{pot}}^{\alpha}(R_0) - E_{\text{kin}}^{\alpha}(T)]$; the roots define R_- and R_+ . *Lower right*: Theoretical nearest neighbor distance at various temperatures.

5. Molecular dynamic simulations

The application of atomistic calculations presented in the previous two sections dealt with ideal crystal lattices. In the following section we will show how to extend the range of applications to arbitrary microstructures by using molecular dynamic simulations.

5.1 Methodology

Molecular dynamics (MD) simulations play an important role in materials science. They are based on the integration of NEWTON's equation of motion and applied in order to understand the dynamic evolution of a system in time. This evolution is driven by the interaction of the particles that enter the equations of motion as forces. In contrast to the quantities calculated in the previous Sections 3 and 4 MD-simulations are particularly useful to obtain quantities that are not accessible directly such as macroscopic diffusion constants or melting temperatures. For an in-depth introduction to MD-simulations we refer the reader to one of the many textbooks (Allen & Tildesley, 1989; Frenkel & Smit, 2001).

The starting point of an MD-simulation is the choice of a thermodynamic ensemble that determines which thermodynamic variables are conserved during the runtime of the simulation. The thermodynamic variables most relevant for applications are temperature T , pressure P , volume V , internal energy E , particle number N and chemical potential μ . The most important ensembles for MD simulations are

- the microcanonical ensemble with constant N, V, E ,
- the canonical ensemble with constant N, V, T , and
- the grand-canonical ensemble with constant μ, V, T .

These macroscopic thermodynamic variables are implicitly included in an atomistic simulation. Their calculation provides a direct link between the macroscopic (system-wide) properties and the microscopic (atom-resolved) MD-simulation. For example, the system-wide instantaneous temperature at a time t is calculated by equipartitioning the kinetic energy of N atoms

$$\frac{1}{2}k_B T(t) = \frac{\sum_{\alpha=1}^N \frac{1}{2}m_{\alpha}[\mathbf{v}_{\alpha}(t) \cdot \mathbf{v}_{\alpha}(t)]}{3N} \quad (56)$$

where m_{α} and \mathbf{v}_{α} are mass and velocity of particle α , respectively. The direct results of an MD-simulation are the positions, velocities and cohesive energies of the system along the simulated trajectory. An example of an NVE simulation is shown in Figure 16: the total energy is constant but the cohesive (i.e. potential) and kinetic energy and the temperature of the system are fluctuating.

The particular choice of ensemble is realised technically by the use of appropriate boundary conditions, thermostats and/or barostats. The variety of available thermostats and barostats differs mainly in the time-reversibility and in the statistic properties. An MD-simulation starts from an initial structure, i.e. atomic positions $\mathbf{X}^{\alpha}(t = 0)$, by calculating the forces on the atoms α . Based on these forces the equations of motion are integrated for a specific timestep δt , i.e. the atomic positions are propagated in time using to new atomic positions $\mathbf{X}^{\alpha}(t + \delta t)$. This is then repeated iteratively (Figure 17), thereby creating the trajectory of the system evolving in time. The propagation of atomic positions in time, based on derivatives of the energy landscape, is an extrapolation with an accuracy that is directly related to the timestep δt . A decrease of δt increases the accuracy of the extrapolation but at the same time decreases

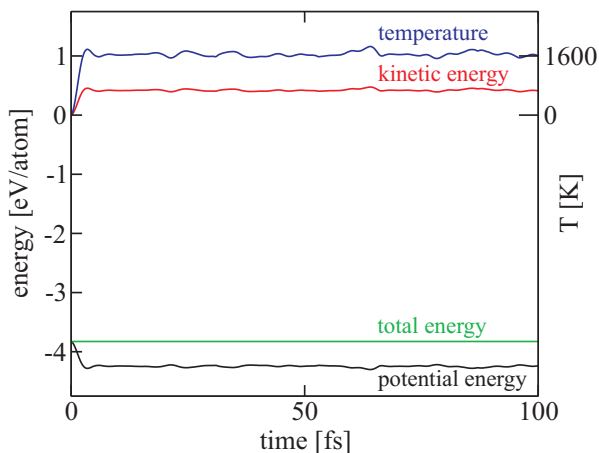


Fig. 16. Time evolution of temperature and energy contributions in an MD-simulation that employs an *NVE* ensemble.

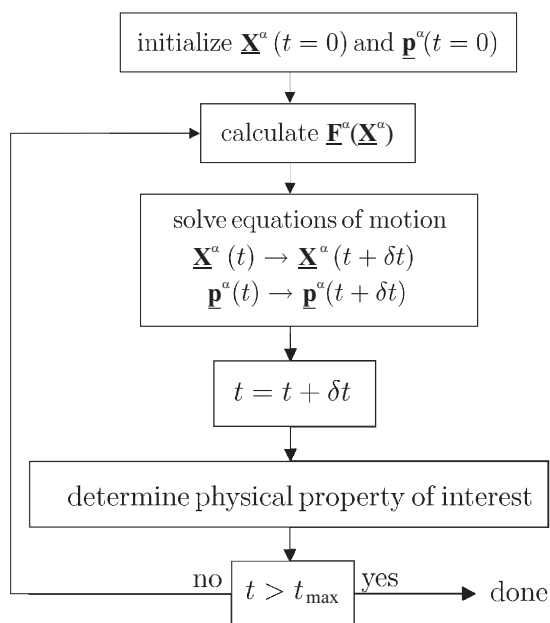


Fig. 17. Flowchart illustrating the principle of a typical MD-simulation.

the simulated system time for a given number of simulation steps. This is overcome by the different integrators that optimise the accuracy of the trajectory for a given number of force and energy calculations per unit system time. A simple approach is the VERLET algorithm that takes the difference of a TAYLOR expansion of the energy for $t - \delta t$ and $t + \delta t$. Then the

terms of even power vanish and one obtains

$$\underline{\mathbf{X}}^\alpha(t + \delta t) = 2\underline{\mathbf{X}}^\alpha(t) - \underline{\mathbf{X}}^\alpha(t - \delta t) + \frac{\underline{\mathbf{F}}^\alpha(t)}{m} \delta t^2 + \mathcal{O}(\delta t^4) \quad (57)$$

as MD-integrator scheme with an error of the order of δt^4 . Due to the absence of velocities in the extrapolation of positions the VERLET algorithm cannot be coupled with thermostats/barostats and hence is suitable for *NVE* ensembles only. Other ensembles can be realised with, e.g., the VELOCITY-VERLET algorithm that involves both, positions and velocities

$$\underline{\mathbf{X}}^\alpha(t + \delta t) = \underline{\mathbf{X}}^\alpha(t) + \underline{\mathbf{v}}^\alpha(t) \delta t + \frac{1}{2} \underline{\mathbf{a}}^\alpha(t) \delta t^2 + \mathcal{O}(\delta t^4) \quad , \quad (58)$$

$$\underline{\mathbf{v}}^\alpha(t + \delta t) = \underline{\mathbf{v}}^\alpha(t) + \frac{1}{2} [\underline{\mathbf{a}}^\alpha(t) + \underline{\mathbf{a}}^\alpha(t + \delta t)] \delta t + \mathcal{O}(\delta t^3) \quad , \quad (59)$$

where $\underline{\mathbf{a}}^\alpha$ denotes the acceleration of atom α . Besides the many other schemes for determining the NEWTONian trajectory (e.g. the NOSE-HOOVER scheme) there are stochastic approaches that aim to explore the phase space of a system instead of following a particular trajectory (LANGEVIN dynamics). Note that these algorithms are independent of the physical approach of the force calculation and purely classical. Treating the dynamics of the system in its full quantum-mechanical character requires more elaborate techniques (Marx & Hutter, 2009).

The structural evolution of the system can be assessed by considering averaged quantities of the atomic positions. The radial distribution function g_2 measures the correlation between the probabilities $\rho(\underline{\mathbf{X}}^\alpha)$ and $\rho(\underline{\mathbf{X}}^{\alpha,*})$ of finding atom β in an infinitesimal volume element at $\underline{\mathbf{X}}^\alpha$ or $\underline{\mathbf{X}}^{\alpha,*}$, respectively, and the probability $\rho(\underline{\mathbf{X}}^\alpha, \underline{\mathbf{X}}^{\alpha,*})$ of finding atoms in both volume elements.

$$\rho(\underline{\mathbf{X}}^\alpha, \underline{\mathbf{X}}^{\alpha,*}) = [\rho(\underline{\mathbf{X}}^\alpha) \rho(\underline{\mathbf{X}}^{\alpha,*})] g_2(\underline{\mathbf{X}}^\alpha, \underline{\mathbf{X}}^{\alpha,*}) \quad (60)$$

This quantity (Figure 18, left) corresponds to measuring the distance-relation between the atoms and provides a good indicator if the system is solid or liquid.

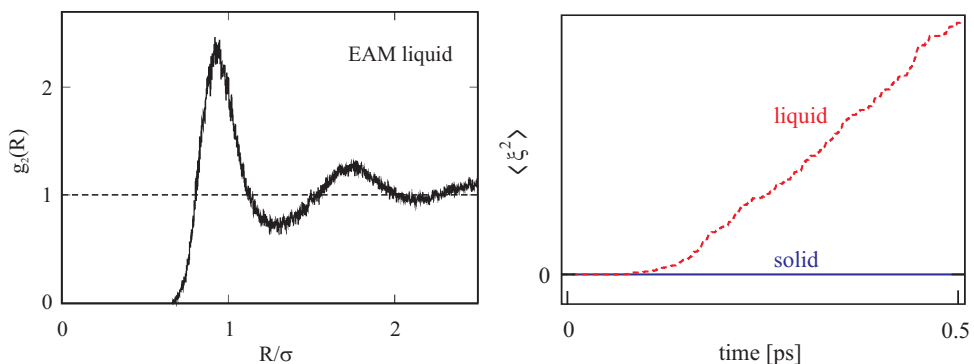


Fig. 18. Radial distribution function (left) and mean square displacement (right) as obtained from an MD simulation (here σ identifies the equilibrium lattice constant).

Another indicator in this direction is the mean square displacement

$$\frac{\partial}{\partial t} \langle \underline{\xi}(t)^2 \rangle = \frac{\partial}{\partial t} \left[\frac{1}{N} \sum_{\beta=1}^N \underline{\xi}^{\beta}(t)^2 \right] = 6D \quad , \quad (61)$$

that relates the microscopic displacements, $\underline{\xi}^{\beta} = \underline{X}^{\beta} - \underline{X}_0^{\beta}$, to the macroscopic diffusion constant D . The time-evolution of this average over atoms gives an indicator of the onset of diffusion in the system. The derivative of the time-evolution of the mean square displacement (Figure 18, right) allows to deduce the macroscopic diffusion constant D . This routinely calculated quantity can be further utilised as input parameters for coarse-grained approaches such as e.g. kinetic Monte-Carlo that is described in detail in e.g. Refs. (Allen & Tildesley, 1989; Frenkel & Smit, 2001).

5.2 Application: Structural transformations

Quantities like the mean-square displacement and the radial distribution function introduced in the previous paragraph provide an overall picture of the system. They are based on atom-averages over quantities which can vary significantly throughout the system. However, such averaging causes loss of information on e.g. a heterogeneous or microstructured system. A technologically important case of a heterogeneous system is a polycrystal that contains crystal grains with different mutual orientations. In some cases the microscopic single-crystal information can be extrapolated to the macroscopic poly-crystalline correspondence, like e.g. the elastic constants (Hill et al., 1963) for randomly distributed grain orientations.

But in the case of structural transformations the spatial variation of the crystal structure and its dependence on time and temperature is the central result of the simulation. This is illustrated by the isolated grain shown in Figure 19 that one of the present authors investigated in the context of growth on microstructured substrates of HCP Titanium. Here, the description of

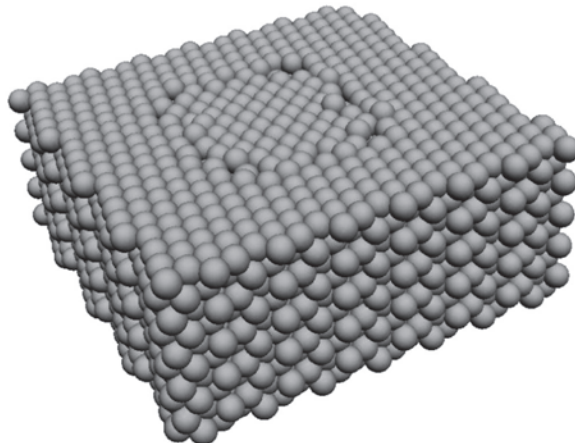


Fig. 19. Isolated grain of HCP Titanium after atomistic relaxation using an embedded-atom potential (Hammerschmidt et al., 2005). The applied angle of misorientation corresponds to a coincidence-site lattice.

interatomic interactions is carried out with an embedded-atom potential described earlier. The parametrisation of the EAM potential was particularly optimised for the description of the undercoordinated atoms at the grain boundary (Hammerschmidt et al., 2005). The atomic structure shown in Figure 19 was obtained by (i) determining the energetically favored atomic structure of the $\Sigma 7(0001)$ coincidence-site lattice (CSL) grain boundary, (ii) setting up a block of CSL cells of orientation A surrounded by cells of orientation B and (iii) relaxing the atoms in the interface area. The atomic relaxation of the interface region did not allow the grain to decay, but resulted in a change of the grain shape from rectangular to nearly circular. Visualising the relaxed grain (Figure 19) along the crystal axis $[1000]$ in Figure 20 allows one to easily distinguish the misoriented grain from the surrounding. In order to investigate the

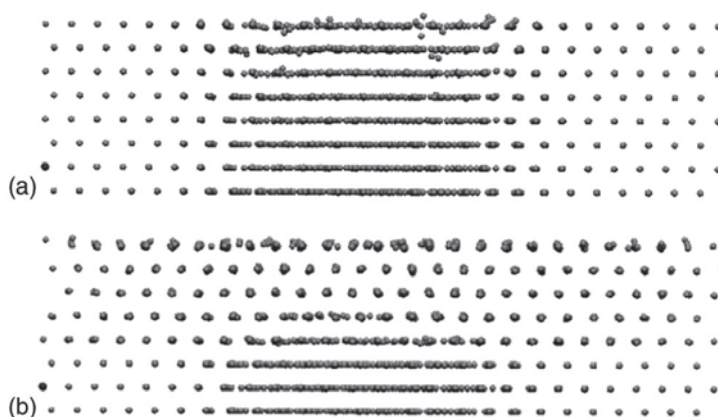


Fig. 20. Initial isolated grain (a), viewed along $[0001]$, undergoes a structural transformation and orients itself to match the surrounding crystal directions (b). The MD-simulation was carried out for 20 ps at 300 K with the bottom three layers fixed, cf. (Hammerschmidt et al., 2005).

structural stability of the isolated grain at elevated temperatures, we carried out molecular dynamic simulations. In particular, we simulated an NVT ensemble for 20 ps at 300 K where we kept the bottom three layers fixed in order to mimic a microstructured substrate. The central finding of this simulation is the decay of the isolated grain within a very short time already at room temperature. Repeating this procedure for isolated grains of different sizes showed that the thermal stability increases with diameter. In particular, we found that grains with a diameter of at least 33\AA are thermally stable over a maximum simulation time of several hundred ps. This compares well with the experimentally observed minimum grain size.

In this example, the analysis of the molecular dynamic simulation is straight-forward. However, simulations of long times and/or large systems make it hard to identify particular events due to the sheer mass of data on atomic trajectories. This calls for approaches that transform the information on atomic positions to meaningful derived atom-based properties like e.g. the moments of the bond-order potentials, Eq. (13), or to even coarse-grained entities like dislocation skeletons (Begau et al., 2011).

6. Summary and outlook

In the foregoing sections various approaches were explained, which allows for the calculation of macroscopic thermodynamic data (e.g. elastic constants, phase stability data, excess enthalpy, heat capacity, and thermal expansion) or mesoscopic material properties (e.g. grain evolution) by using atomistic calculation methods. Starting with the quantum-mechanical SCHRÖDINGER equation and ending with various empirical potentials a brief hierarchical overview was given, which describes different precise possibilities to quantify atomic interactions. Subsequently, the EAM-framework was applied to derive energy expressions for the pure solid and binary alloys. Once the energy is calculated investigations of static and dynamic (vibrations) lattice deformations as well as thermodynamic and thermo-mechanical materials behaviour can be performed. For this reason different, technologically relevant materials were investigated such as Fe-C, Ag, Cu, and the binary brazing alloy Ag-Cu. In order to analyze the thermodynamics of many particle systems (such as diffusion) statistical ensembles and mean quantities (e.g. the mean displacement) were finally considered, which are derived, for example, via MD-simulations. In particular, MD-calculations were presented, which allow to predict the temporal evolution of different grain orientations in "polycrystalline" Titanium.

The presented methods can help to overcome many difficulties related to the determination of material parameters on the mesoscopic length scale. Note that there are already many examples - beyond the present work - for the successful applications of atomistic calculations to gain information about the materials behavior on micro- or macroscale, see e.g. (Begau et al., 2011; Bleda et al., 2008; Chiu et al., 2008; Kadau et al., 2004) or (Bian et al., 2008; Böhme et al., 2007; Williams et al., 2006), respectively. Two, recently published, examples are worth mentioning: calculations of the interaction of hydrogen with voids and grain boundaries in steel under the allowance of different alloying elements, (Nazarov et.al., 2010), and investigations of the influence of hydrogen on the elastic properties of α -iron, (Psiachos et al., 2011).

Nevertheless, the bridging of length- and timescales is still a big challenge for most multiscale approaches. Here information of the nano- (e.g. binding energies of different H-traps, such as dislocations and phase boundaries) and microscale (e.g. the temporal and spatial phase distribution in multiphase materials) must be incorporated in macroscopic, constitutive equations (e.g. the diffusion equation with source/sink-term for hydrogen trapping, (McNabb & Foster, 1963; Oriani, 1970)). Moreover, the ongoing increase of computational capacities and the development of suitable interfaces for considering atomistic or microstructural calculations in commercial simulation software will further establish multiscale approaches in materials engineering. The FE^2 -method, for instance, described by (Balzani et.al., 2010) shows the large potential for incorporating micro- or mesoscopic information in macroscopic simulations, but also the need for further acceleration of numerical calculations and the development of optimized algorithms.

7. References

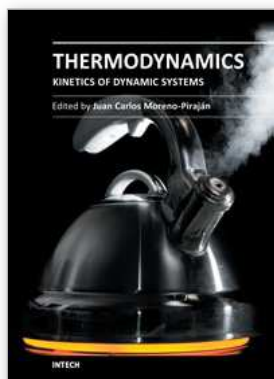
- Abell, G.C. (1985). Empirical chemical pseudopotential theory of molecular and metallic bonding, *Phys. Rev. B*, Vol. 31, 6184–6196 (and references therein).
- Alinaghian, P.; Gumbsch, P.; Skinner, A.J. & Pettifor, D.G. (1993). Bond order potentials: a study of s- and sp-valent systems, *J. Phys.: Cond. Mat.*, Vol. 5, 5795–5810.

- Allen, M.P. & Tildesley, D.J. (1989). *Computer simulation of liquids*, Oxford University Press, ISBN: 019-8-55645-4, New York.
- Aoki, M.; Nguyen-Manh, D.; Pettifor, D.G. & Vitek, V. (2007). Atom-based bond-order potentials for modelling mechanical properties of metals. *Prog. Mat. Sci.*, Vol. 52, 154–195.
- Artemev, A.; Wang, Y. & Khachaturyan, A.G. (2000). Three-dimensional phase field model and simulation of martensitic transformation in multilayer systems under applied stresses, *Acta Mater.*, Vol. 48, 2503–2518.
- Balzani, D. & Schröder, J. & Brands, D. (2010). FE²-Simulation of Microheterogeneous Steels Based on Statistically Similar RVE's, In: *IUTAM Symposium on Variational Concepts with Applications to the Mechanics of Materials*, Hackl K. (Ed.), IUTAM Bookseries, Vol. 21, 15–28, Springer, ISBN: 978-90-481-9195-6, Dordrecht Heidelberg London New York.
- Bangwei, Z.; Yifang, O.; Shuzhi, L. & Zhanpeng, J. (1999). An analytic MEAM model for all BCC transition metals. *Physica B*, Vol. 262, 218–225.
- Baskes, M.I. (1992). Modified embedded-atom potentials for cubic materials and impurities. *Phys. Rev. B*, Vol. 46, 2727–2742.
- Begau, C.; Hartmaier, A.; George, E.P. & Pharr, G.M. (2011). Atomistic processes of dislocation generation and plastic deformation during nanoindentation. *Acta Materialia*, Vol. 59, 934–942.
- Behler, J. & Parrinello, M. (2007). Generalized Neural-Network Representation of High-Dimensional Potential-Energy Surfaces. *Phys. Rev. Lett.*, Vol. 98, No. 14, 146401–146404.
- Bian, Q.; Bose, S.K. & Shukla, R.C. (2008). Vibrational and thermodynamic properties of metals from a model embedded-atom potential. *J. Phys. Chem. Solids*, Vol. 69, 168–181.
- Bleda, E.A.; Gao, X. & Daw, M.S. (2008). Calculations of diffusion in FCC binary alloys using on-the-fly kinetic Monte Carlo. *Comp. Mat. Sci.*, Vol. 43, 608–615.
- Bockstedte, M.; Kley, A.; Neugebauer, J. & Scheffler, M. (1997). Density-functional theory calculations for poly-atomic systems: electronic structure, static and elastic properties and ab initio molecular dynamics, *Comp. Phys. Comm.*, Vol. 107, 187–222.
- Böhme, T.; Dreyer, W. & Müller, W.H. (2007). Determination of stiffness and higher gradient coefficients by means of the embedded-atom method - an approach for binary alloys. *Continuum Mech. Therm.*, Vol. 18, 411–441.
- Born, M. & Oppenheimer, R. (1927). Zur Quantentheorie der Molekeln, *Ann. Phys.*, Vol. 84, 457–484.
- Cahn, J.W. (1968). Spinodal decomposition. *Trans. Metall. Soc. AIME*, Vol. 242, 166–180.
- Cryot-Lackmann, F. (1967). On the electronic structure of liquid transition metals. *Adv. Phys.*, Vol. 16, 393–400.
- Daw, M.S. & Baskes, M.I. (1983). Semiempirical, quantum mechanical calculation of hydrogen embrittlement in metals. *Phys. Rev. Lett.*, Vol. 50, 1285–1288.
- Daw, M.S. & Baskes, M.I. (1984). Embedded-atom method: derivation and application to impurities, surfaces and other defects in metals. *Phys. Rev. B*, Vol. 29, 6443–6453.
- De Fontaine, D. (1975). Clustering effects in solid solutions, In: *Treatise in solid state chemistry*, Vol. 5: *Changes of state*, N. B. Hannay (Ed.), 129–178, Plenum, New-York.
- Desai, S.K.; Neeraj, T. & Gordon, P.A. (2010). Atomistic mechanism of hydrogen trapping in bcc Fe-Y solid solution: A first principles study, *Acta Mater.*, Vol. 58, 5363–5369.

- Chiu, J.-T.; Lin, Y.-Y.; Shen, C.-L.; Lo, S.-P. & Wu, W.-J. (2008). Atomic-scale finite-element model of tension in nanoscale thin film, *Int. J. Adv. Manuf. Technol.*, Vol. 37, 76–82.
- Drautz R. & Pettifor, D.G. (2006). Valence-dependent analytic bond-order potential for transition metals, *Phys. Rev. B*, Vol. 74, 174117/1–174117/14.
- Drautz, R.; Zhou, X.W.; Murr, D.A.; Gillespie, B.; Wadley, H.N.G. & Pettifor, D.G. (2007). Analytic bond-order potentials for modelling the growth of semiconductor thin films, *Prog. Mat. Sci.*, Vol. 52, 196–229.
- Dreizler, R.M. & Gross, E.K.U. (1990). *Density Functional Theory*, Springer, ISBN: 3-540-51993-9, Berlin.
- Feraoun, H.; Aourag, H.; Grosdidier, T.; Klein, D. & Coddet, C. (2001). Development of modified embedded atom potentials for the Cu-Ag system. *Superlattice Microst.*, Vol. 30, No. 5, 261–271.
- Finnis, M.W. & Sinclair, J.E. (1984). A simple empirical N-body potential for transition metals, *Phil. Mag. A*, Vol. 50, 45–55.
- Finnis, M.W. (2007a). Bond-order potentials through the ages. *Prog. Mat. Sci.*, Vol. 52, 133–153.
- Finnis, M.W. (2007b). *Interatomic forces in condensed matter*. Oxford University Press, ISBN: 978-0-19-50977-6, New York.
- Foiles, S.M.; Baskes, M.I. & Daw, M.S. (1986). Embedded-atom-method functions for the fcc metals Cu, Ag, Au, Ni, Pd, Pt, and their alloys. *Phys. Rev. B*, Vol. 33, 7983–7991.
- Fornasini, P.; Beccara, S. a; Dalba, G.; Grisenti, R.; Sanson, A. & Vaccari, M. (2004). Extended x-ray-absorption fine-structure measurements of copper: Local dynamics, anharmonicity, and thermal expansion. *Phys. Rev. B*, Vol. 70, 174301/1–174301/12.
- Frenkel, D. & Smit, B.J. (2001). *Understanding Molecular Simulation: From Algorithms to Applications*, Academic Press Inc., ISBN: 012-2-67370-0, Orlando, FL, USA.
- Hammerschmidt, T.; Kersch, A. & Vogl, P. (2005). Embedded atom simulations of titanium systems with grain boundaries. *Phys. Rev. B*, Vol. 71, 205409/1–205409/9.
- Hammerschmidt, T.; Seiser, B.; Drautz, R. & Pettifor, D.G. (2008). *Modelling topologically close-packed phases in superalloys: Valence-dependent bond-order potentials based on ab-initio calculations*, in: *Superalloys 2008*, edited by R. C. Reed (The Metals, Minerals and Materials Society, Warrendale), 847–853.
- Hammerschmidt, T. & Drautz, R. (2009). Bond-Order Potentials for Bridging the Electronic to Atomistic Modelling Hierarchies. in: *NIC Series 42 - Multiscale Simulation Methods in Molecular Science*, edited by J. Grotendorst, N. Attig, S. Blügel and D. Marx. (Jülich Supercomputing Centre, 2009), 229–246.
- Hammerschmidt, T.; Drautz, R. & Pettifor, D.G. (2009). Atomistic modelling of materials with bond-order potentials. *Int. J. Mat. Res.*, Vol. 100, 1479–1487.
- Hill, R. (1963). Elastic properties of reinforced solids - Some theoretical principles. *J. Mech. Phys. Solids*, Vol. 11, 357–372.
- Hohenberg, P. & Kohn, W. (1964). Quantum density oscillations in an inhomogeneous electron gas, *Phys. Rev.*, Vol. 137, A1697–A1705.
- Horsfield, A.; Bratkovsky, A.M.; Fearn, M.; Pettifor, D.G. & Aoki, M. (1996). Bond-order potentials: Theory and implementation, *Phys. Rev. B*, Vol. 53, 12694–12712.
- Hristova, E.; Janisch, R.; Drautz, R. & Hartmaier, A. (2011). Solubility of carbon in α -iron under volumetric strain and close to the $\Sigma 5(310)[001]$ grain boundary: Comparison of DFT and empirical potentials, *Comp. Mat. Sci.*, Vol. 50, 1088–1096.
- Johnson, R.A. (1972). Relationship between two-body interatomic potentials in a lattice model and elastic constants. *Phys. Rev. B*, Vol. 6, 2094–2100.

- Johnson, R.A. (1974). Relationship between two-body interatomic potentials in a lattice model and elastic constants II. *Phys. Rev. B*, Vol. 9, 1304–1308.
- Johnson, R.A. (1988). Analytic nearest-neighbor model for FCC metals. *Phys. Rev. B*, Vol. 37, 3924–3931.
- Johnson, R.A. (1989). Alloy model with the embedded-atom-method. *Phys. Rev. B*, Vol. 39, 12554–12559.
- Jones, J.E. (1924). On the Determination of Molecular Fields. II. From the Equation of State of a Gas, *Proc. R. Soc. Lond. A*, Vol. 106, No. 738, 463–477.
- Kadau, K.; German, T.C.; Lomdahl, P.S.; Holian, B.L.; Kadau, D.; Entel, P.; Kreth, M.; Westerhoff, F. & Wolf, D.E. (2004). Molecular-Dynamics Study of Mechanical Deformation in Nano-Crystalline Aluminum, *Metall. Mater. Trans. A*, Vol. 35A, 2719–2723.
- Kagaya, H.-M.; Shoji, N. & Soma, T. (1988). Anharmonic effects on the thermal properties of Si and Ge. *Solid State Commun.*, Vol. 65, No. 11, 1445–1450.
- Kittel, C. (1973). *Einführung in die Festkörperphysik* (3. erweiterte und verbesserte Auflage), R. Oldenbourg Verlag GmbH München Wien, John Wiley & Sons GmbH, Frankfurt, ISBN: 978-3-486-32763-2.
- Kobayashi, R.; Warren, J.A. & Carter, W.C. (2000). A continuum model of grain boundaries. *Physica D*, Vol. 140, 141–150.
- Kohn, W. & Sham, L.J. (1965). Self-consistent equations including exchange and correlation effects, *Phys. Rev.*, Vol. 140, A1133–A1138.
- Kohn, W. (1998). An essay on condensed matter physics in the twentieth century, *Rev. Mod. Phys.*, Vol. 71, S59–S77.
- Lee, B.-J. (2006). A modified embedded-atom method interatomic potential for the Fe-C system, *Acta Mater.*, Vol. 54, 701–711.
- Lee, B.-J. & Jang, J.-W. (2007). A modified embedded-atom method interatomic potential for the Fe-H system, *Acta Mater.*, Vol. 55, 6779–6788.
- Leibfried, G. (1955). Mechanische und thermische Eigenschaften der Kristalle, In: *Handbuch der Physik. Band VII*, S. Flügge (Ed.), 104–324, Springer, Berlin-Göttingen-Heidelberg.
- Marx, D. & Hutter, J. (2009). *Ab-Initio Molecular Dynamics: Basic Theory And Advanced Methods*, Cambridge University Press, ISBN: 978-0-521-89863-8, Cambridge.
- McNabb, A. & Foster, P.K. (1963). A New Analysis of the Diffusion of Hydrogen in Iron and Ferritic Steels. *Trans. Metall. Soc. AIME*, Vol. 227, 618–627.
- Mrovec, M.; Nguyen-Manh, D.; Pettifor, D.G. & Vitek, V. (2004). Bond-order potential for molybdenum: Application to dislocation behaviour. *Phys. Rev. B*, Vol. 69, 094115/1–094115/16.
- Mrovec, M.; Moseler, M.; Elsässer, C. & Gumbsch, P. (2007). Atomistic modeling of hydrocarbon systems using analytic bond-order potentials, *Prog. Mat. Sci.*, Vol. 52, 230–254.
- MTDATA NPL database for materials thermochemistry (1998). Queens Road, Teddington, Middlesex, TW11 0LW.
- Najafabadi, R.; Srolovitz, D.J.; Ma, E. & Atzmon, M. (1993). Thermodynamic properties of metastable Ag-Cu alloys. *J. Appl. Phys.*, Vol. 74, No. 5, 3144–3149.
- Nazarov, R. & Hickel, T. & Neugebauer, J. (2010). First-principles study of the thermodynamics of hydrogen-vacancy interaction in fcc iron. *Phys. Rev. B*, Vol. 82, No. 22, 224104/1–224104/11

- Oriani, R.A. (1970). The diffusion and trapping of hydrogen in steel. *Acta Metall.*, Vol. 18, 147–157.
- Parr, R.G. & Yang, W. (1989). *Density-Functional Theory of Atoms and Molecules*, Oxford University Press, ISBN: 978-0-195-09276-9, New York.
- Payne, M.C.; Teter, M.P.; Allen, D.C.; Arias, T.A. & Joannopoulos, J.D. (1992). Iterative minimization techniques for ab initio total-energy calculations: molecular dynamics and conjugate gradients, *Rev. Mod. Phys.*, Vol. 64, 1045–1097.
- Pettifor, D.G. (1989). New many-body potential for the bond-order, *Phys. Rev. B*, Vol. 63, 2480–2483.
- Pettifor, D.G. & Oleinik, I.I. (1999). Analytic bond-order potentials beyond Tersoff-Brenner. I. Theory, *Phys. Rev. B*, Vol. 59, 8487–8499.
- Pettifor, D.G. & Oleinik, I.I. (2000). Bounded Analytic Bond-Order Potentials for σ and π Bonds. *Phys. Rev. Lett.*, 84, 4124–4127.
- Psiachos, D.; Hammerschmidt, T. & Drautz, R. (2011). Ab initio study of the modification of elastic properties of α -iron by hydrostatic strain and by hydrogen interstitials. *Acta Mater.*, Vol. 59, 4255–4263.
- Rose, J.H.; Smith, J.R.; Guinea, F. & Ferrante, J. (1984). Universal features of the equation of state of metals. *Phys. Rev. B*, Vol. 29, 2963–2969.
- Stølen, S. & Grande, T. (2003). *Chemical thermodynamics of materials - macroscopic and microscopic aspects*, John Wiley & Sons Ltd, ISBN: 0 471 49230 2, Chichester West Sussex, England.
- Sutton, A.P.; Finnis, M.W.; Pettifor, D.G. & Ohta, Y. (1988). The tight-binding bond model. *J. Phys. C*, Vol. 21, 35–66.
- Svensson, E.C.; Brockhouse, B.N. & Rowe, J.M. (1984). Crystal Dynamics of Copper. *Phys. Rev.*, Vol. 155, 619–632.
- Tersoff, J. (1986). New empirical model for the structural properties of silicon. *Phys. Rev. Lett.*, Vol. 56, 632–635.
- van Duin, A.C.T.; Dasgupta, S.; Lorant, F. & Goddard, W.A. (2001). ReaxFF: A reactive force field for hydrocarbons. *J. Phys. Chem. A*, Vol. 105, No. 41, 9396–9409.
- Wallace, D.C. (1965). Thermal Expansion and other Anharmonic Properties of Crystals. *Phys. Rev.*, Vol. 139, No. 3A, A877–A888.
- Williams, P.L.; Mishin, Y. & Hamilton, J.C. (2006). An embedded-atom potential for the Cu-Ag system. *Model. Simul. Mater. Sc.*, Vol. 14, 817–833.
- Yu, P.Y. & Cardona, M. (2010). *Fundamentals of Semiconductors - Physics and Materials Properties*, Springer, ISBN: 978-3-642-00710-1, Berlin Heidelberg.
- Zhang, J.-M.; Wang, D.-D. & Xu, K.-W. (2006). Calculation of the surface energy of hcp metals by using the modified embedded atom method. *Appl. Surf. Sci.*, Vol. 253, 2018–2024.



Thermodynamics - Kinetics of Dynamic Systems

Edited by Dr. Juan Carlos Moreno Piraján

ISBN 978-953-307-627-0

Hard cover, 402 pages

Publisher InTech

Published online 22, September, 2011

Published in print edition September, 2011

Thermodynamics is one of the most exciting branches of physical chemistry which has greatly contributed to the modern science. Being concentrated on a wide range of applications of thermodynamics, this book gathers a series of contributions by the finest scientists in the world, gathered in an orderly manner. It can be used in post-graduate courses for students and as a reference book, as it is written in a language pleasing to the reader. It can also serve as a reference material for researchers to whom the thermodynamics is one of the area of interest.

How to reference

In order to correctly reference this scholarly work, feel free to copy and paste the following:

T. Böhme, T. Hammerschmidt, R. Drautz and T. Pretorius (2011). Closing the Gap Between Nano- and Macroscale: Atomic Interactions vs. Macroscopic Materials Behavior, Thermodynamics - Kinetics of Dynamic Systems, Dr. Juan Carlos Moreno Piraján (Ed.), ISBN: 978-953-307-627-0, InTech, Available from: <http://www.intechopen.com/books/thermodynamics-kinetics-of-dynamic-systems/closing-the-gap-between-nano-and-macroscale-atomic-interactions-vs-macroscopic-materials-behavior>

INTech

open science | open minds

InTech Europe

University Campus STeP Ri
Slavka Krautzeka 83/A
51000 Rijeka, Croatia
Phone: +385 (51) 770 447
Fax: +385 (51) 686 166
www.intechopen.com

InTech China

Unit 405, Office Block, Hotel Equatorial Shanghai
No.65, Yan An Road (West), Shanghai, 200040, China
中国上海市延安西路65号上海国际贵都大饭店办公楼405单元
Phone: +86-21-62489820
Fax: +86-21-62489821

© 2011 The Author(s). Licensee IntechOpen. This chapter is distributed under the terms of the [Creative Commons Attribution-NonCommercial-ShareAlike-3.0 License](#), which permits use, distribution and reproduction for non-commercial purposes, provided the original is properly cited and derivative works building on this content are distributed under the same license.